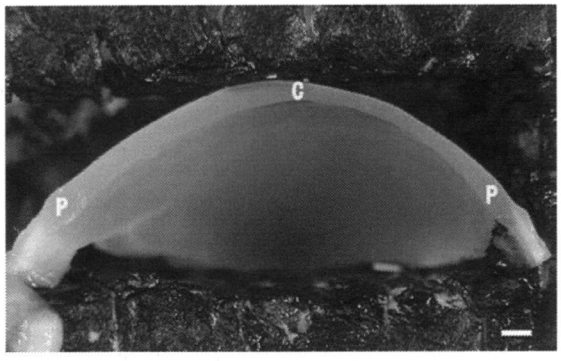

Fig. 1. A photograph showing the median plane of the cornea. Apparently, the central portion (C) is thinner than the peripheral portion (P). Scale bar=1 mm.

difference between the number of collagen lamellae in the central portion (253 ± 49 lamellae) and that in the peripheral portion (236 ± 22 lamellae). Collagen lamellae in the central portion (796.2 ± 426.9 nm) tended to be thinner than those in the peripheral portion (1,113.5 ± 562.9 nm) (Fig. 2). CFI of the central portion (29.1 ± 3.8 nm and 39.0 ± 4.9%) were significantly lower than those of the peripheral portion (32.6 ± 3.5 nm and 41.6 ± 4.8%) (Fig. 2). These results were summarized in Table 1.

The difference between thickness of the central portion and that of the peripheral portion of the cornea in the beagle dog is somewhat consistent with that found in other species [1, 17, 18]. Such a site-dependent difference appears to be attributable to the difference in thickness of the substantia propria, which occupies a large ratio of the cornea. The substantia propria is an important area for light passing through in the cornea. In the corneal substantia propria, collagen fibril diameter at the central portion was approximately 10% smaller than that at the peripheral portion, and CFI was also significantly lower at the central portion than at the peripheral portion by approximately 5%. These factors appeared to be responsible for the difference in thickness of the collagen lamellae, which reflected the difference in corneal thickness.

The difference in collagen fibril diameter would reflect difference in the composition ratio of collagen molecular species and proteoglycans [2, 3, 7, 15, 20]. Furthermore, the amount and types of proteoglycans could affect the arrangement and density of collagen fibrils [8, 9]. Collagen from both corneal portions was therefore extracted and site-dependent difference in the composition ratio of collagen molecular species was determined. As a result, type I (α2) to type V (α1) collagen ratios in both portions were approximately 75:25. In addition, ratios of decorin to lumican in the central portion and the peripheral portion were 1:0.64 and 1:0.74, respectively (unpublished data). Although there was no apparent site-dependent difference in the composition ratio of collagen molecular species, the amount of decorin and lumican, the two major proteoglycans accumulated in the corneal substantia propria, were found to be larger at

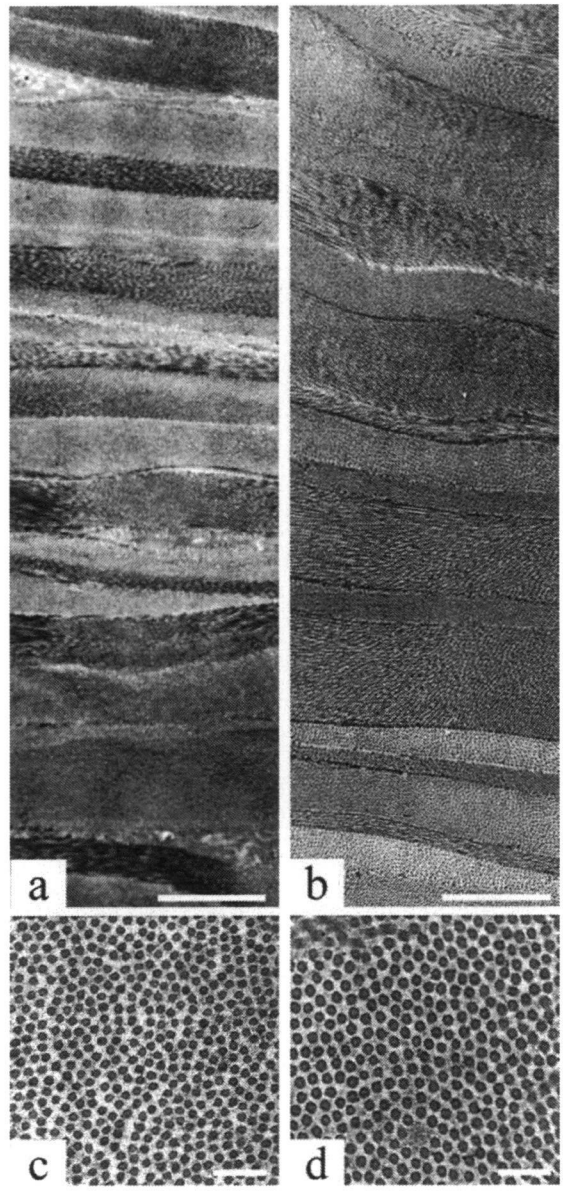

Fig. 2. Transmission electron micrographs showing collagen lamellae and collagen fibrils in the central portion and peripheral portion of the corneal substantia propria. Collagen lamellae in the central portion (a) are thinner but more abundant than those in the peripheral portion (b). Diameter of collagen fibrils in the central portion (c) appeared to be smaller than that in the peripheral portion (d) of the cornea. Scale bars=2 μm (a, b) and 200 nm (c, d).

the central portion than at the peripheral portion. Both proteoglycans have been shown to inhibit an increase in collagen fibril diameter and regulate fibrillar spacing [4, 9, 15]. Therefore, the larger accumulation of proteoglycans in the central portion may be important for the production of many small diameter collagen fibrils, resulting in thinness of the

Table 1. Morphological comparison of the central and peripheral portions of the cornea

Measurements	Central portion	Peripheral portion
Entire corneal thickness (mm)	540.8 ± 205.5*	724.6 ± 178.3
Thickness ratio of substantia propria to entire cornea (%)	86.2	86.5
Number of collagen lamellae	253 ± 49	236 ± 22
Thickness of collagen lamellae (nm)	796.2 ± 426.9	1113.5 ± 562.9
Collagen fibril diameter (nm)	29.1 ± 3.8*	32.6 ± 3.5
Collagen fibril index (CFI) (%)	39.0 ± 4.9*	41.6 ± 4.8

Values are means ± SD.
*Significantly different from peripheral cornea ($p<0.05$).

entire cornea. The central portion of the cornea was abundant in the collagen fibrils of small diameter, which have been shown to prevent slippage between collagen fibrils and thereby impart their elasticity [10, 12–14, 16]. Since the cornea covers the anterior part of the eyeball and constitutes the outmost layer of the eyeball, these fibrils may also buffer the direct impact of intraocular pressure on the central portion of the cornea. The peripheral portion of the corneal substantia propria was abundant in the collagen fibrils of large diameter, which are characterized by high-density intermolecular crosslink to provide a strong resistance to tensile force [10, 12–14, 16]. Because the periphery of the cornea continues with the sclera [1, 18], the abundance of collagen fibrils with large diameter in the substantia propria of this portion would also provide a strong resistance to tensile force from the adjacent sclera. The present study has revealed that the site-dependent difference in the cornea is closely associated with function and maintenance of the unique shape of the eyeball.

REFERENCES

1. Anthony, J. B., Ramesh, C. T. and Brenda, J. T. 1997. The cornea and sclera. pp. 233–278. *In*: Wolff's Anatomy of the Eye and Orbit, 8th ed., Chapman & Hall, London.
2. Birk, D. E., Fitch, J. M., Babiarz, J. P., Doane, K. J. and Linsenmayer, T. F. 1990. Collagen fibrillogenesis *in vitro*: interaction of types I and V collagen regulates fibril diameter. *J. Cell Sci.* **95**: 649–657.
3. Birk, D. E. and Mayne, R. 1997. Localization of collagen types I, III and V during tendon development. Changes in collagen types I and III are correlated with changes in fibril diameter. *Eur. J. Cell Biol.* **72**: 352–361.
4. Danielson, K. G., Baribault, H., Holmes, D. F., Graham, H., Kadler, K. E. and Iozzo, R. V. 1997. Targeted disruption of decorin leads to abnormal collagen fibril morphology and skin fragility. *J. Cell Biol.* **136**: 729–743.
5. Flint, M. H., Craig, A. S., Reilly, H. C. and Parry, D. A. 1984. Collagen fibril diameters and glycosaminoglycan content of skins-indices of tissue maturity and function. *Connect. Tissue Res.* **13**: 69–81.
6. Gerhard, K. L. 2007. Cornea, pp. 115–159. *In*: Ophthalmology, 2nd ed., Thieme, New York.
7. Iozzo, R. V. 1997. The family of the small leucine-rich proteoglycans: key regulators of matrix assembly and cellular growth. *Crit. Rev. Biochem. Mol. Biol.* **32**: 141–174.
8. Iwasaki, S., Hosaka, Y., Iwasaki, T., Yamamoto, K., Nagayasu, A., Ueda, H., Kokai, Y. and Takehana, K. 2008. The modulation of collagen fibril assembly and its structure by decorin: an electron microscopic study. *Arch. Histol. Cytol.* **71**: 37–44.
9. Kao, W. W. and Liu, C. Y. 2002. Roles of lumican and keratocan on corneal transparency. *Glycoconj. J.* **19**: 275–285.
10. Magnusson, S. P., Hansen, P. and Kjaer, M. 2003. Tendon properties in relation to muscular activity and physical training. *Scand. J. Med. Sci. Sports* **13**: 211–223.
11. Nagayasu, A., Hosaka, Y., Yamasaki, A., Tsuzuki, K., Ueda, H., Honda, T. and Takehana, K. 2008. A preliminary study of direct application of atelocollagen into a wound lesion in the dog cornea. *Curr. Eye Res.* **33**: 727–735.
12. Parry, D. A. 1988. The molecular and fibrillar structure of collagen and its relationship to the mechanical properties of connective tissue. *Biophys. Chem.* **29**: 195–209.
13. Parry, D. A., Barnes, G. R. and Craig, A. S. 1978. A comparison of the size distribution of collagen fibrils in connective tissues as a function of age and a possible relation between fibril size distribution and mechanical properties. *Proc. R. Soc. Lond. B. Biol. Sci.* **203**: 305–321.
14. Parry, D. A., Craig, A. S. and Barnes, G. R. 1978. Tendon and ligament from the horse: an ultrastructural study of collagen fibrils and elastic fibres as a function of age. *Proc. R. Soc. Lond. B. Biol. Sci.* **203**: 293–303.
15. Rada, J. A., Cornuet, P. K. and Hassell, J. R. 1993. Regulation of corneal collagen fibrillogenesis *in vitro* by corneal proteoglycan (lumican and decorin) core proteins. *Exp. Eye Res.* **56**: 635–648.
16. Raspanti, M., Ottani, V. and Ruggeri, A. 1990. Subfibrillar architecture and functional properties of collagen: a comparative study in rat tendons. *J. Anat.* **172**: 157–164.
17. Raviola, E. 1994. THE EYE. pp. 872–918. *In*: A Textbook of Histology, 12th ed. (Fawcett, D. W. and Raviola, E. eds.), Chapman & Hall, New York.
18. Samuelson, D. A. 1991. Ophthalmic embrology and anatomy. pp. 3–123. *In*: Veterinary Ophthalmology, 2nd ed., (Gellat, K.N. ed.), Lea and Febiger, Philadelphia.
19. Sumide, T., Nishida, K., Yamato, M., Ide, T., Hayashida, Y., Watanabe, K., Yang, J., Kohno, C., Kikuchi, A., Maeda, N., Watanabe, H., Okano, T. and Tano, Y. 2006. Functional human corneal endothelial cell sheets harvested from temperature-responsive culture surfaces. *FASEB J.* **20**: 392–394.
20. Takemura, Y., Mizuno, K., Imamura, Y. and Hayashi, T. 2003. Preferential liberation of type V collagen from bovine corneal stroma by limited treatment with proteases. *Connective Tissue* **35**: 133–139.
21. Tsuzuki, K., Yamashita, K., Izumisawa, Y. and Kotani, T. 2008. Microstructure and glycosaminoglycan ratio of canine cornea after reconstructive transplantation with glycerin-preserved porcine amniotic membranes. *Vet. Ophthalmol.* **11**: 222–227.

TISSUE ENGINEERING: Part C
Volume 00, Number 00, 2009

DOI: 10.1089/ten.tec.2009.0459

Development of a New Assay System for Evaluating the Permeability of Various Substances Through Three-Dimensional Tissue

Yuji Haraguchi, Ph.D.,[1,*] Waki Sekine, M.Sc.,[1,*] Tatsuya Shimizu, M.D., Ph.D.,[1,*] Masayuki Yamato, Ph.D.,[1] Shunichiro Miyoshi, M.D., Ph.D.,[2] Akihiro Umezawa, M.D., Ph.D.,[3] and Teruo Okano, Ph.D.[1]

A novel assay system with cell-dense three-dimensional (3D) tissue was developed for measuring the permeability of substances. In this paper, the permeabilities of various molecules containing nutrients, a cytokine, and a chemokine were examined and analyzed. A single-layered cell sheet was approximately 20 μm thick, and as the number of layers of these cell sheets increased, so did the total thickness of the tissue. The diffusion rates of glucose and pyruvic acid were reduced to approximately 30–40% by a single-layered cell sheet compared with the control without the cell sheet, and the diffusion of both substances were completely inhibited by a quadruple-layered cell sheet. The diffusion rate of creatinin was reduced to approximately 50% and 15–20% by a single-layered and by a quintuplet-layered cell sheet, respectively. On the other hand, the diffusion rate of stromal cell–derived factor 1α, vascular endothelial growth factor, β2-microglobulin, and transferrin was reduced to approximately 10%, 5%, 20%, and 10%, by only a single-layered cell sheet, respectively. The diffusion of these substances were completely inhibited by a double-layered cell sheet. These results show that the permeability of substances through 3D tissue significantly decreased with the increase of the molecular weight. Therefore, the system could give a simulated living-tissue condition for measuring the permeability of substances. To our knowledge, this is the first report about measuring the permeability of substances through cell-dense 3D tissues without scaffolds. The assay system is believed to contribute to the progress of physiology, metabolism, biochemistry, and pharmacokinetics. Further, the system may give some hints for developing a new dialysis membrane technology for an artificial kidney.

Introduction

THERE ARE MANY REPORTS that described the adverse effects, the permeability, and the uptakes of various substances, including nutrients and drugs, by *in vitro* cell assay systems, which were designed and used model systems for the heart tissue, the small intestinal mucosa, the oral mucosa, the blood–brain barrier, the blood–retinal barrier, and so on.[1–6] These assay systems are essential in the field of pharmacokinetics as well as in the understanding of biochemistry, physiology, and metabolism of tissues and organs. An adequate assay system has a clear advantage as *in vitro* models that could require no animal experiments. To date, experiments in these fields have relied on assays using two-dimensional (2D) single-layered cell cultures. Two-dimensional culture system is too simple in comparison with actual living tissues or organs. Cells of 2D culture system are significantly different from that of three-dimensional (3D) culture system in terms of their morphology, cell-to-cell interactions, surrounding extracellular matrix, proliferation rates, and differentiation.[7–9] These differences may affect their gene expression and other biological activities. It is believed that 3D culture system can simulate *in vivo* situations.[7,10,11] An *in vitro* assay system using 3D tissues would, therefore, be clearly desirable in the fields described above.

Three-dimensional tissues can be re-constructed *in vitro* using tissue engineering techniques.[12] Conventional tissue engineering has employed 3D scaffolds (e.g., polyglycolic acid, collagen gel, and gelatin) that are useful as alternatives for extracellular matrix, and cells are seeded into the scaffolds. However, 3D tissues fabricated by using the scaffolds are extremely cell-sparse tissues because of insufficient cell migration into the scaffolds.[13,14] In an attempt to improve this situation, our laboratory has created and utilized an original

[1]Institute of Advanced Biomedical Engineering and Science, TWIns, Tokyo Women's Medical University, Tokyo, Japan.
[2]Department of Cardiology, Keio University School of Medicine, Tokyo, Japan.
[3]Department of Reproductive Biology and Pathology, National Research Institute for Child Health and Development, Tokyo, Japan.
*These three authors contributed equally to this study.

technology called cell sheet engineering,[15] which can prepare 3D tissues without the scaffolds by layering cell sheets harvested from temperature-responsive culture dishes.[16–19] This method allows cell harvest to require no proteolytic treatments and to preserve cell-to-cell connections completely.[20,21] The technique also can control the thickness of re-constructed 3D tissues by manipulating the number of cell layers. Therefore, 3D tissues fabricated by the cell sheet engineering are suitable as an *in vitro* cell-dense 3D tissue model.

In this study, we develop a new assay system that uses cell-dense 3D tissues made by the cell sheet engineering in conjunction with a modified cell culture insert, and measured the permeability of various substances, including nutrients, a cytokine, and a chemokine, through the cell-dense 3D tissues for verifying the usefulness of the system.

Materials and Methods

Culture of C2C12 mouse skeletal myoblast cell lines and human endometrial gland–derived mesenchymal cells

C2C12 mouse skeletal myoblast cell lines were purchased from Dainippon Sumitomo Pharma (Osaka, Japan). C2C12 cells and human endometrial gland–derived mesenchymal cells (EMCs)[22] were cultured in Dulbecco's modified Eagle's medium (DMEM; Sigma-Aldrich Japan, Tokyo) supplemented with 10% fetal bovine serum (Japan Bio Serum, Nagoya, Japan) and 1% penicillin and streptomycin (Invitrogen, Carlsbad, CA). These cells were cultured at 37°C in a humidified atmosphere with 5% CO_2.

A device for permeability experiments

A device was developed by modifying a cell culture insert (the membrane pore size: 3 μm; Becton, Dickinson and Company, Franklin Lakes, NJ) as shown in Fig. 1. Briefly, a round polyethylene terephthalate film (diameter: 30 mm) having a hole in its center (diameter: 5 mm) was glued to the outside-bottom of the membrane of the cell culture insert with cyanoacrylate adhesive (Toagosei, Tokyo, Japan) (Fig. 1). A single cell sheet or a several layered cell sheet was then placed on the bottom of the device, covering the permeance hole, as described in detail below (Fig. 2A–E). Thus, substances in the upper medium could diffuse only through the cell sheets and the permeance hole.

Preparation of cell sheets and the manipulation of the cell sheets into layered constructs

Cell suspensions were plated onto a 35 mm temperature-responsive culture dish (Upcell; CellSeed, Tokyo, Japan) at 6×10^5 cells/dish (for C2C12 cells) or 1×10^6 cells/dish (for EMCs). After 3 days (C2C12 cells) or 4 days (EMCs), the culture dishes were placed in a separate CO_2 incubator set at 20°C. Each cell sheet with its medium was gently aspirated into a tip of a pipette and put on the bottom membrane of the device one at a time. An additional medium was then poured into the upper part of the device, having the cell sheet for spreading out any folded portions. Once the cell sheet was spread out, the medium was aspirated away, and the device was incubated for 60 min at 37°C to allow the cell sheet to fully adhere to the bottom membrane of the device. Cell sheets were layered by repeating the following procedure: detaching another cell sheet from a temperature-responsive culture dish and stacking it onto the first cell sheet. In this manner, triple-, quadruple-, and quintuple-layered constructs were created. After 60 min incubation, a fresh medium was added to the device's upper and lower parts, and the device was incubated at 37°C for 24 h. Upon the end of the incubation, the culture media of the upper and lower parts were separately collected and were used for chemical and protein analyses, and enzyme-linked immunosorbent assay (ELISA). The volumes of the upper and lower media were also measured.

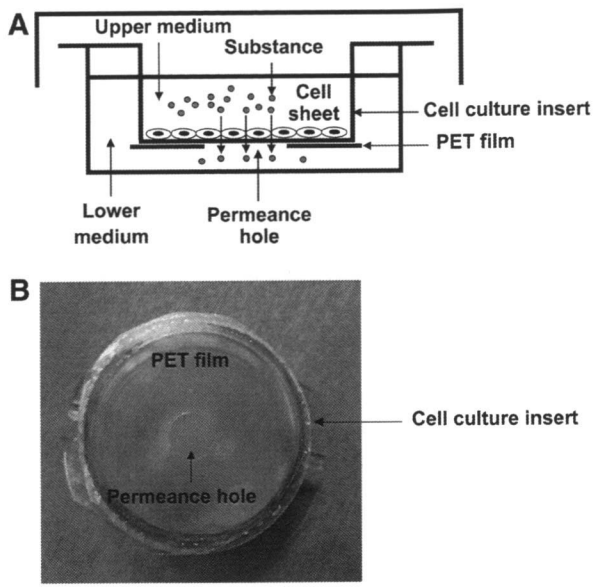

FIG. 1. A device to measure the permeability of substances. A schematic illustration of the device as viewed from the side is shown in (**A**). (**B**) is a photograph as viewed from the bottom.

Histological analysis

Cell sheets on the device were fixed with 4% paraformaldehyde. Specimens were embedded in paraffin, sectioned, and stained with hematoxylin and eosin. Prepared specimens were examined by a microscope (Elipse TE2000-U; Nikon, Tokyo, Japan).

Medium, chemical, and proteins

Glucose/pyruvic acid–deficient DMEM was purchased from Invitrogen; creatinin, human β2-microglobulin, and human transferrin were from Wako Pure Chemicals (Tokyo, Japan); human vascular endothelial growth factor (VEGF) and human stromal–derived factor 1α (SDF-1α) were from Funakoshi (Tokyo, Japan).

Chemical and protein analyses, and ELISA

Concentrations of glucose, pyruvic acid, and creatinin were measured by the hexokinase UV method,[23] the pyruvate oxidase method,[24] and an enzymatic method by SRL (Tokyo, Japan), respectively. Concentrations of β2-microglobulin and transferrin were measured by a latex agglutination test (SRL).

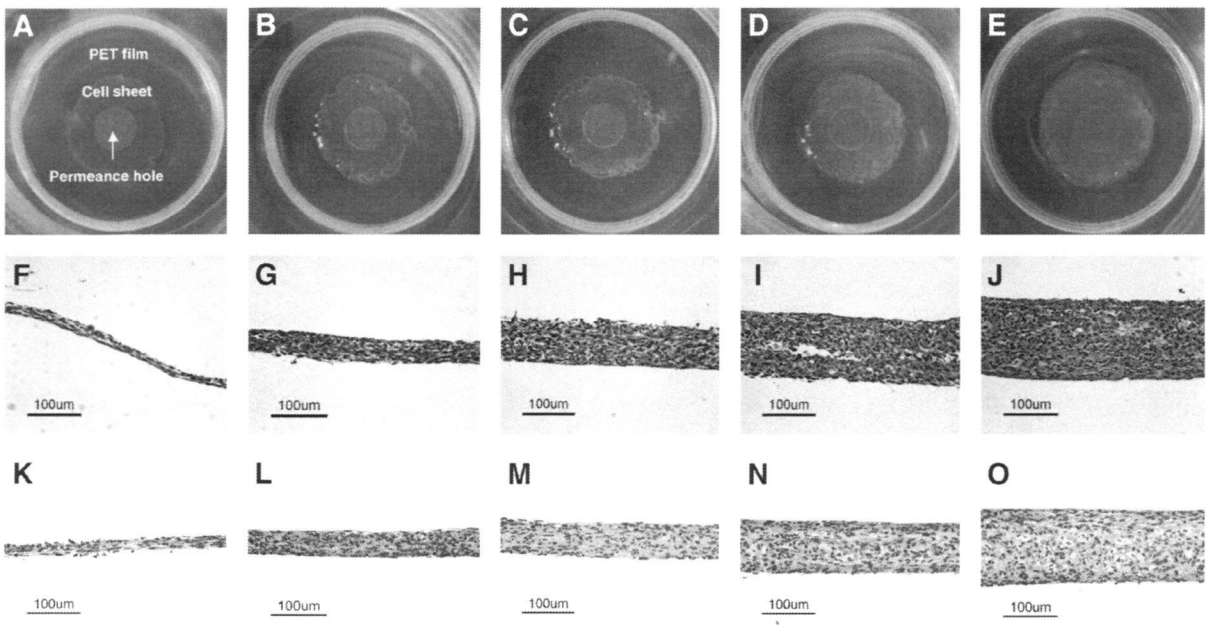

FIG. 2. Morphological and histological observation of single cell sheets and of cell sheets with several layers. The photograph (**A**) shows a monolayer EMC sheet on a new device; (**B**), a double-layered EMC sheet; (**C**), a triple-layered EMC sheet; (**D**), a quadruple-layered EMC sheet; and (**E**), a quintuplet-layered EMC sheet. Cross-sectional observation of layered C2C12 cell sheets (**F–J**) and EMC sheets (**K–O**). Photographs (**F**) and (**K**) show single-layered cell sheets; (**G**) and (**L**), double-layered cell sheets; (**H**) and (**M**), triple-layered cell sheets; (**I**) and (**N**), quartet-layered cell sheets; (**J**) and (**O**), quintet-layered cell sheets. Scale bars indicate 100 μm.

Amounts of human VEGF and SDF-1α were quantitated by a commercially available ELISA kit (Funakoshi).

Relative permeability and relative residual amount of each substance

Permeability of each substance was calculated by the following equation:

$$\text{Permeability} = \frac{\text{The concentration of a substance in the lower medium}}{\text{The volume of the lower medium}} \times 100$$

For comparison, the permeability of a substance without a cell sheet was assumed to be 100% (the control permeability), and its relative permeability through a cell sheet was calculated by the following equation:

$$\text{Relative permeability} = \frac{\text{The permeability of a substance through a cell sheet}}{\text{The control permeability}} \times 100$$

The residual amount of a substance was calculated by the following equation:

Residual amount = [the amount of a substance remaining in the upper medium after incubation for 24 h] + [the amount of a substance in the lower medium after incubation for 24 h].

The residual amount without the cell sheet was estimated at 100% (the control residual amount). Relative residual amounts were then calculated for substances by the following equation:

$$\text{Relative residual amount} = \frac{\text{The residual amount of a substance for 24 h with cell sheet}}{\text{The control residual amount}} \times 100$$

Data are expressed as mean ± SD.

Results

Morphologic analysis of cell sheets

The cross sections of single-layered and multi-layered cell sheets were observed. When the culture temperature was decreased from 37°C to 20°C, C2C12 cells or EMCs on a temperature-responsive culture dish were detached as a contiguous cell sheet. Those cell sheets shrunk horizontally due to the cytoskeletal tensile reorganization. As a result, those cell sheets consisted of two or three cell layers, and the thickness of the cell sheets became approximately 20 μm (Fig. 2F, K). The addition of a layered cell sheet to a tissue increased the total tissue's thickness by the thickness of the added cell sheet (Fig. 2F–J, the C2C12 cell sheet; Fig. 2K–O, the EMC sheet). These results show that cell sheet engineering can control the thickness of 3D tissues.

Permeability of the substances through layered cell sheets

Because nutrients (pyruvic acid and glucose) are vital for living tissues, the permeability through the 3D tissue is a basic factor for tissue engineering. Therefore, our first experiments assessed the permeability of the nutrients through

C2C12 cell sheets by adding DMEM into the upper section of the device and glucose/pyruvic acid–deficient DMEM into the lower part. The permeabilities of pyruvic acid and glucose were inhibited by approximately 60% (in other words, it was reduced to approximately 40%) by a single-layered C2C12 cell sheet (Fig. 3A, B). As the number of layered cell sheets increased, the permeabilities of pyruvic acid and glucose decreased. Almost complete inhibition of the permeability was observed upon the use of a quadruple-layered or a quintuple-layered cell sheet (Fig. 3A, B). Similar results were also observed using EMC sheets (Fig. 3D, E).

In the next set of experiments, the permeabilities of creatinin, β2-microgloblin, and transferrin were examined, because these are important substances for measuring the kidney glomerulus function.[25,26] DMEM containing creatinin, β2-microglobulin, or transferrin was added to the upper part of the device, while DMEM without these substances was added to the lower part. The permeability of creatinin was inhibited by approximately 50% by a single-layered C2C12 cell sheet (Fig. 3C). Again, as the number of layered cell sheets increased, the sheets' collective inhibitory effects increased. The permeability of creatinin was inhibited by approximately 85% by a quintuple-layered cell sheet (Fig. 3C). On the other hand, the permeabilities of β2-microglobulin and transferrin were inhibited by approximately 80% and 90% by only a single-layered C2C12 cell sheet, respectively, and both were almost completely inhibited by a double-layered cell sheet (Fig. 4A, B). Similar results were also observed using EMC sheets (Figs. 3F and 4D, E).

In the third set of experiments, the permeabilities of VEGF and SDF-1α were examined, because these substances are important in the regeneration of tissues.[27,28] DMEM containing either SDF-1α or VEGF was added to the upper part of the device, while DMEM was added to the lower part. C2C12 cells secreted SDF-1α, and EMCs secreted VEGF, but not SDF-1α (data not shown). A human-specific VEGF ELISA kit, which is unable to cross react with mouse VEGF, was used to detect VEGF. Therefore, only C2C12 cell sheets were used for determining the permeability of VEGF, and only EMC sheets were used for determining the permeability of SDF-1α. The permeability of VEGF was inhibited by approximately 95% (in other words, it was reduced to 5%) by a single-layered C2C12 cell sheet and was almost completely inhibited by a double-layered cell sheet (Fig. 4C). Likewise, the permeability of SDF-1α was inhibited by approximately 90% by a single-layered EMC sheet and was almost completely inhibited by a double-layered cell sheet (Fig. 4F).

The rate of consumption of glucose and pyruvic acid increased as the number of cell sheets increased. Once tissues had more than triple-layered cell sheets, the increase of the rate slowed (Fig. 5A, B). Similar tendency was also observed in the experiments using EMC sheets (Fig. 5C, D). In contrast, the amount of creatinin, SDF-1α, VEGF, β2-microglobulin, and transferrin was hardly changed during incubation with layered cell sheets (data not shown).

Discussion

Many reports have already been published regarding the permeability and uptake of various substances through a single-layered of cells.[1–5] The present study is unique and original because our new assay system can measure the permeability of substances through cell-dense 3D tissues rather than a single-layered of cells. The cell-dense 3D tissue was prepared by cell sheet engineering, and the device was made by our laboratory.

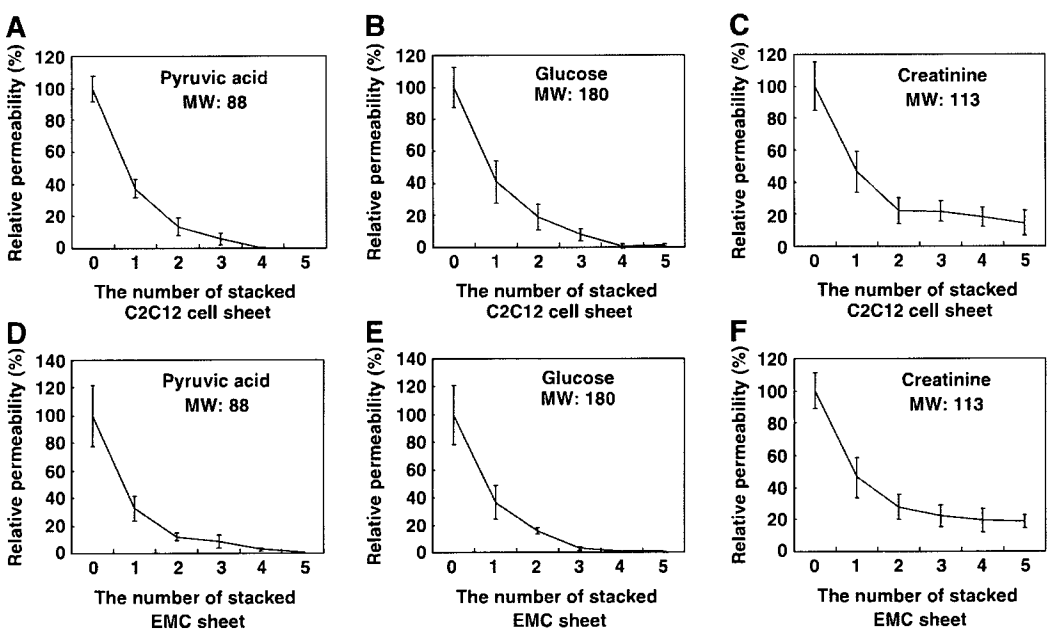

FIG. 3. Permeability of low-molecular-weight substances. The graph (**A**) shows pyruvic acid experiment through C2C12 cell sheets; (**B**), glucose; and (**C**), creatinin. The graph (**D**) shows pyruvic acid experiment through EMC sheets; (**E**), glucose; and (**F**), creatinin. The data are expressed as mean ± SD ($n = 4$).

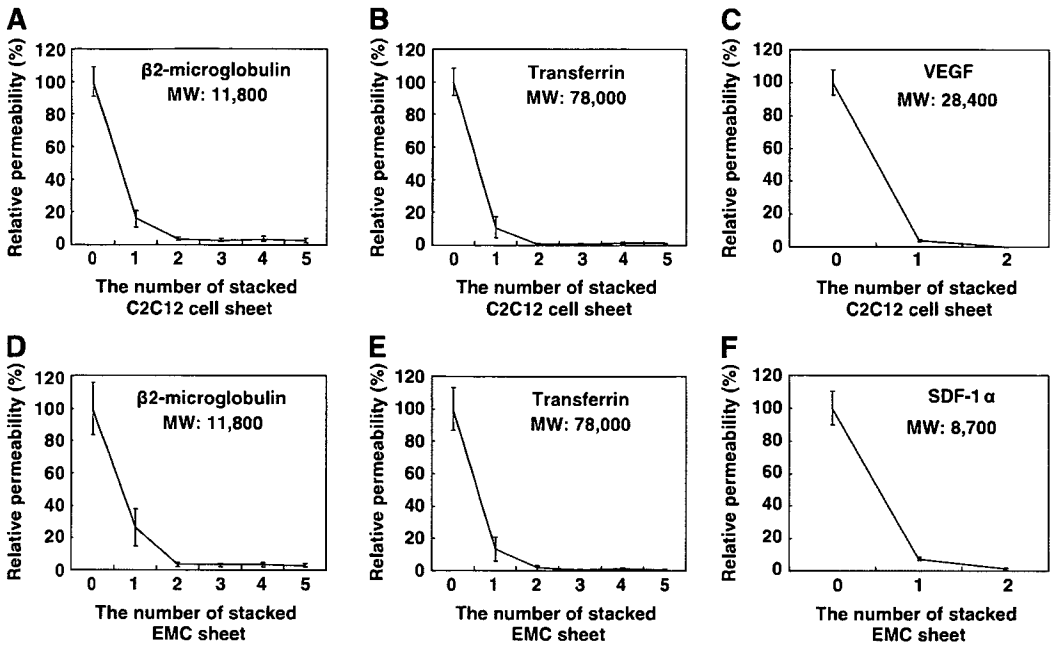

FIG. 4. Permeability of high-molecular-weight substances. The graph (A) shows β2-microglobulin experiment through C2C12 cell sheets; (B), transferrin; and (C), VEGF. The graph (D) shows β2-microglobulin experiment through EMC sheets; (E), transferrin; and (F), SDF-1α. The data are expressed as mean ± SD ($n = 4$).

First, we used our assay system to examine the permeability of nutrients across 3D tissues (Fig. 3). The results suggested that the cells that were separated from their nutrient source by more than triple-layered cell sheets were severely starved of nutrients. Both *in vivo* and *in vitro*, cell death was found to be common in engineered tissues of more than triple-layered cell sheets, though the same kinds of cells usually survive without necrosis in tissues consisting of a single-, a double-, or a triple-layered cell sheet[29] (Sekine, W., Haraguchi, Y., Shimizu, T., Umezawa, A., and Okano, T.,

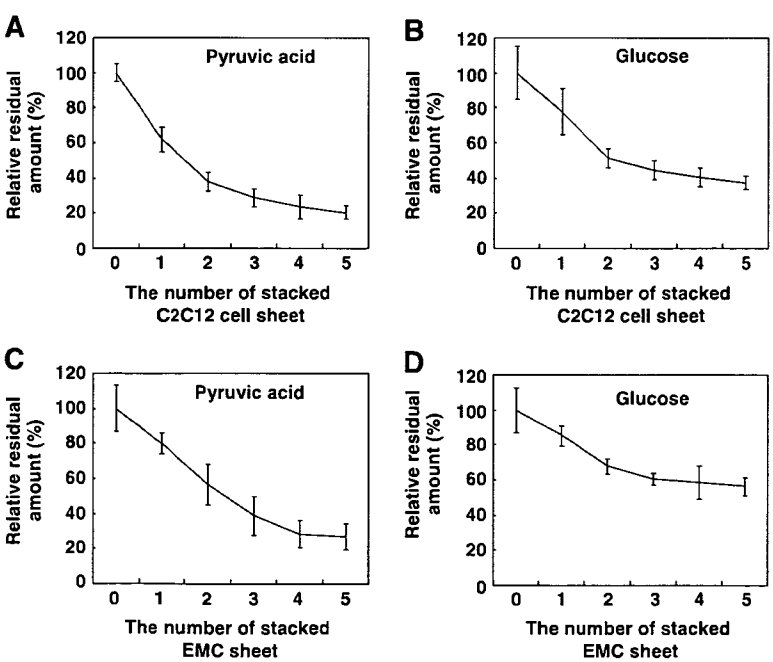

FIG. 5. Consumption of nutrients during incubation with layered cell sheets. The graph (A) shows relative residual amount of pyruvic acid after incubation with C2C12 cell sheets, and (B) shows that of glucose. The graph (C) shows relative residual amount of pyruvic acid after incubation with EMC sheets, and (D) shows that of glucose. The amounts of substances taken after 24 h without the cell sheet were assumed to be 100%. The data are expressed as mean ± SD ($n = 4$).

unpublished observation). Our results suggested that insufficient diffusion of nutrients induces a rapid cell death in the thick tissues. Other reports, in contrast, have claimed that glucose could penetrate into 3D tissues via a scaffold containing skeletal muscle myoblasts.[30] The report showed that glucose concentrations only decreased from 4.28 mmol/L at the edge of the tissue to 3.18 mmol/L at the depth of 2 mm.[30] This result is profoundly different from ours; the inconsistency is probably due to different cell densities of 3D tissues of the two studies. In this study, 3D tissues, which were fabricated by cell sheet engineering, were constructed without 3D scaffolds described above and were, therefore, very cell dense. In contrast, in the reported study, 3D tissues fabricated using scaffolds were very cell sparse due to insufficient cell migration into the scaffolds. Nevertheless, both our study and that of Davis *et al.*[30] present important data that are relevant to the field of tissue metabology.

In another set of experiments, the permeability of high-molecular-weight substrates (SDF-1α, VEGF, β2-microglobulin, and transferrin) was completely inhibited by a double-layered cell sheet. These results show that cells in tissues that are only one or two layers thick can be deficient in growth factors or cytokines. We propose that the formation of functional microvessels is necessary to supply these large molecules into the interiors of 3D tissues. On the other hand, VEGF and SDF-1α have received a great deal of attention from the field of regenerative medicine.[27,28] The former is intimately involved in angiogenesis, and the latter with stem cell homing. In fact, VEGF has even been used in clinical therapy, and in animal experiment; SDF-1α could improve myocardial function after infarction.[26,28] It is thought that the effectiveness of these factors depends on the efficiency of diffusion into the treated area. In the present study, we showed that these factors were unable to diffuse efficiently into the cell-dense tissues. Thus, the successful implementation of cytokine therapy will require a development of techniques that can help these factors diffuse efficiently. Our assay system using cell-dense 3D tissues may be useful for the development of efficient cytokine therapy.

In this article, the permeability of substances through cell-dense 3D tissue was shown to be significantly reduced depending on the molecular weight (Figs. 3 and 4). This observation agrees with a report that the permeability of mannitol (molecular weight: 182) through a single-layered of brain capillary endothelial cell lines on a cell culture insert was approximately twice as great as that of inulin (molecular weight: 5,000).[2] These results showed that the permeability of substances through 2D cell culture and 3D tissues was significantly reduced with the increase of molecular weight, and that our assay system is feasible as an assay system to measure the permeability of substances through 3D tissues.

Drug development requires the development of *in vitro* assay systems that simulate actual living tissues and organs. In addition, an adequate assay system has a clear advantage as an *in vitro* model that require no animal experiments. The researcher should try as much as possible to replace the animal model with an alternative nonanimal model.[31] It is generally thought that 3D culture systems resemble *in vivo* situations much more closely than 2D culture systems.[7,10,11] Cell sheet engineering gives the fabrication of cell-dense 3D tissues without biodegradable scaffolds. Therefore, for example, layered cardiomyocyte sheets interact directly with each other and can couple electrically, resulting in synchronously beating 3D myocardial tissues *in vitro*.[32,33] *In vivo* subcutaneous transplantation of layer cardiomyocyte sheets also demonstrated that these synchronously beating heart-like tissues survive for over 1 year.[33] Our *in vitro* 3D assay system using cell sheet engineering is thought to be proper for *in vivo* situation. Therefore, our assay system has potential to reduce animal experiment. In addition, the cell sheet engineering also enables the fabrication of complicated heterogeneous tissues. In fact, our laboratory previously reported about heterogeneous 3D coculture comprising hepatocytes and endothelial cells using the technique.[34] The hepatocytes of the 3D culture system showed a differentiated cell shape and the extensive albumin expression of hepatocytes, which were never seen in hepatocyte monoculture.[34] Combination of our assay system and heterogeneous layering cell sheets can allow us to analyze pharmacologically and pharmacokinetically complicated 3D tissues such as the blood–brain barrier, the small intestinal mucosa, and the kidney glomerulus. For example, the blood–brain barrier model can be fabricated by a combination of an endothelial cell sheet, a pericyte sheet, and an astrocyte sheet.

Several novel therapies containing a hybrid bioartificial kidney for the treatment of kidney failure are tried clinically.[35] The hybrid bioartificial kidney is combined with dialysis membrane and cells. In this study a device by modifying a cell culture insert was used. By the replacement of the device dialysis membrane and cell sheet, a new hybrid-type artificial kidney model device can also be fabricated easily. Therefore, our assay system may be applied in the field of dialysis membrane technology.

Conclusions

We have developed a new model system that measures the permeability of substances through cell-dense 3D tissues using cell sheet engineering and a modified cell culture insert, and analyzed in detail the permeability of various molecules. It has been shown that our assay system is feasible as an assay system to measure the permeability of substances through 3D tissues using substances that have various molecular weights. This is the first report about measuring the permeability of substances through cell-dense 3D tissues without scaffolds. The thickness of the tissues can be also controlled easily as shown in Figure 2. Our assay system represents a significant advancement and offers much exciting potential in the fields of biochemistry, physiology, metabology of tissues, cytokine therapy, drug development, and dialysis membrane technology.

Acknowledgments

We appreciate the useful comments and technical criticism of Drs. Norio Ueno and Noriaki Matsuda (Institute of Advanced Biomedical Engineering and Science, Tokyo Women's Medical University). This work was supported by grants from the 21COE program and the High-Tech Research Center Program from the Ministry of Education, Culture, Sports, Science, and Technology; grants from the Japan Society for the Promotion of Science; Research Grants for Cardiovascular Disease and Regenerative Medicine from the

Ministry of Health, Labour, and Welfare; and the Open Research Grant from the Japanese Research Promotion Society for Cardiovascular Diseases.

Disclosure Statement

No competing financial interests exist.

References

1. Hilgers, A.R., Conradi, R.A., and Burton, P.S. Caco-2 cell monolayers as a model for drug transport across the intestinal mucosa. Pharm Res **7,** 902, 1990.
2. Hosoya, K., Tetsuka, K., Nagase, K., Tomi, M., Saeki, S., Ohtsuki, S., Takanaga, H., Yanai, N., Obinata, M., Kikuchi, A., Okano, T., and Terasaki, T. Conditionally immortalized brain capillary endothelial cell lines established from a transgenic mouse harboring temperature-sensitive simian virus 40 large T-antigen gene. AAPS Pharm Sci **2,** E27, 2000.
3. Kimura, T., Yamano, H., Tanaka, A., Matsumura, T., Ueda, M., Ogawara, K., and Higaki, K. Transport of D-glucose across cultured stratified cell layer of human oral mucosal cells. J Pharm Pharmacol **54,** 213, 2002.
4. Roux, F., and Couraud, P.O. Rat brain endothelial cell lines for the study of blood-brain barrier permeability and transport functions. Cell Mol Neurobiol **25,** 41, 2005.
5. Tomi, M., Terayama, T., Isobe, T., Egami, F., Morito, A., Kurachi, M., Ohtsuki, S., Kang, Y.S., Terasaki, T., and Hosoya, K. Function and regulation of taurine transport at the inner blood-retinal barrier. Microvasc Res **73,** 100, 2007.
6. Mukhopadhyay, P., Rajesh, M., Bátkai, S., Kashiwaya, Y., Haskó, G., Liaudet, L., Szabó, C., and Pacher, P. Role of superoxide, nitric oxide, and peroxynitrite in doxorubicin-induced cell death *in vivo* and *in vitro*. Am J Physiol Heart Circ Physiol **296,** 1466, 2009.
7. Abbott, A. Biology's new dimension. Nature **424,** 870, 2003.
8. Brännvall, K., Bergman, K., Wallenquist, U., Svahn, S., Bowden, T., Hilborn, J., and Forsberg-Nilsson, K. Enhanced neuronal differentiation in a three-dimensional collagen-hyaluronan matrix. J Neurosci Res **85,** 2138, 2007.
9. Liu, H., Collins, S.F., and Suggs, L.J. Three-dimensional culture for expansion and differentiation of mouse embryonic stem cells. Biomaterials **27,** 6004, 2006.
10. Editorial. Goodbye, flat biology? Nature **424,** 861, 2003.
11. Smalley, K.S., Lioni, M., and Herlyn, M. Life isn't flat: taking cancer biology to the next dimension. In Vitro Cell Dev Biol Anim **42,** 242, 2006.
12. Langer, R., and Vacanti, J.P. Tissue engineering. Science **260,** 920, 1993.
13. Leor, J., Aboulafia-Etzion, S., Dar, A., Shapiro, L., Barbash, I.M., Battler, A., Granot, Y., and Cohen, S. Bioengineered cardiac grafts: a new approach to repair the infracted myocardium? Circulation **100(suppl II),** II63, 1999.
14. Sakai, T., Li, R.K., Weisel, R.D., Mickle, D.A., Kim, E.T., Jia, Z.Q., and Yau, T.M. The fate of a tissue-engineered cardiac graft in the right ventricular outflow tract of the rat. J Thorac Cardiovasc Surg **121,** 932, 2001.
15. Yamato, M., and Okano, T. Cell sheet engineering. Materials Today **7,** 42, 2004.
16. Yamada, N., Okano, T., Sakai, H., Karikusa, F., Sawasaki, Y., and Sakurai, Y. Thermo-responsive polymeric surface: control of attachment and detachment of cultured cells. Makromol Chem Rapid Commun **11,** 571, 1990.
17. Okano, T., Yamada, N., Sakai, H., and Sakurai, Y. A novel recovery system for cultured cells using plasma-treated polystyrene dishes grafted with poly (N-isopropylacrylamide). J Biomed Mater Res **27,** 1243, 1993.
18. Yang, J., Yamato, M., Shimizu, T., Sekine, H., Ohashi, K., Kanzaki, M., Ohki, T., Nishida, K., and Okano, T. Reconstruction of functional tissues with cell sheet engineering. Biomaterials **28,** 5033, 2007.
19. Matsuda, N., Shimizu, T., Yamato, M., and Okano, T. Tissue engineering based on cell sheet technology. Adv Mater **19,** 3089, 2007.
20. Yamato, M., Utsumi, M., Kushida, A., Konno, C., Kikuchi, A., and Okano, T. Thermo-responsive culture dishes allow the intact harvest of multilayered keratinocyte sheets without dispase by reducing temperature. Tissue Eng **7,** 473, 2001.
21. Nishida, K., Yamato, M., Hayashida, Y., Watanabe, K., Maeda, N., Watanabe, H., Yamamoto, K., Nagai, S., Kikuchi, A., Tano, Y., and Okano, T. Functional bioengineered corneal epithelial sheet grafts from corneal stem cells expanded *ex vivo* on a temperature-responsive cell culture surface. Transplantation **77,** 379, 2004.
22. Hida, N., Nishiyama, N., Miyoshi, S., Kira, S., Segawa, K., Uyama, T., Mori, T., Miyado, K., Ikegami, Y., Cui, C., Kiyono, T., Kyo, S., Shimizu, T., Okano, T., Sakamoto, M., Ogawa, S., and Umezawa, A. Novel cardiac precursor-like cells from human menstrual blood-derived mesenchymal cells. Stem Cells **26,** 1695, 2008.
23. Koch, C.D. Determination of glucose with glucoseoxidase-UV, using hexokinase as the reference method. J Clin Chem Clin Biochem **14,** 373, 1976.
24. Valero, E., and García-Carmona, F. Optimizing enzymatic cycling assays: spectrophotometric determination of low levels of pyruvate and L-lactate. Anal Biochem **239,** 47, 1996.
25. Boron, W.F., and Boulpaep, E.L. Medical Physiology. Philadelphia, PA: Elsevier Science, 2003.
26. Branten, A.J., Swinkels, D.W., Klasen, I.S., and Wetzels, J.F. Serum ferritin levels are increased in patients with glomerular diseases and proteinuria. Nephrol Dial Transplant **19,** 2754, 2004.
27. Tang, J., Wang, J., Song, H., Huang, Y., Yang, J., Kong, X., Guo, L., Zheng, F., and Zhang, L. Adenovirus-mediated stromal cell-derived factor-1 alpha gene transfer improves cardiac structure and function after experimental myocardial infarction through angiogenic and antifibrotic actions. Mol Biol Rep (in press).
28. Gaffney, M.M., Hynes, S.O., Barry, F., and O'Brien, T. Cardiovascular gene therapy: current status and therapeutic potential. Br J Pharmacol **152,** 175, 2007.
29. Shimizu, T., Sekine, H., Yang, J., Isoi, Y., Yamato, M., Kikuchi, A., Kobayashi, E., and Okano, T. Polysurgery of cell sheet grafts overcomes diffusion limits to produce thick, vascularized myocardial tissues. FASEB J **20,** 708, 2006.
30. Davis, B.H., Schroeder, T., Yarmolenko, P.S., Guilak, F., Dewhirst, M.W., and Taylor, D.A. An *in vitro* system to evaluate the effects of ischemia on survival of cells used for cell therapy. Ann Biomed Eng **35,** 1414, 2007.
31. Vitale, A., Manciocco, A., and Alleva, E. The 3R principle and the use of non-human primates in the study of neurodegenerative diseases: the case of Parkinson's disease. Neurosci Biobehav Rev **33,** 33, 2009.
32. Shimizu, T., Yamato, M., Isoi, Y., Akutsu, T., Setomaru, T., Abe, K., Kikuchi, A., Umezu, M., and Okano T. Fabrication of

pulsatile cardiac tissue grafts using a novel 3-dimensional cell sheet manipulation technique and temperature-responsive cell culture surfaces. Circ Res **90,** e40, 2002.
33. Shimizu, T., Yamato, M., Kikuchi, A., and Okano, T. Cell sheet engineering for myocardial tissue reconstruction. Biomaterials **24,** 2309, 2003.
34. Harimoto, M., Yamato, M., Hirose, M., Takahashi, C., Isoi, Y., Kikuchi, A., and Okano, T. Novel approach for achieving double-layered cell sheets co-culture: overlaying endothelial cell sheets onto monolayer hepatocytes utilizing temperature-responsive culture dishes. J Biomed Mater Res **62,** 464, 2002.
35. Fissell, W.H. Developments towards an artificial kidney. Expert Rev Med Devices **3,** 155, 2006.

Address correspondence to:
Teruo Okano, Ph.D.
Institute of Advanced Biomedical Engineering and Science
TWIns, Tokyo Women's Medical University
8-1 Kawada-cho, Shinjuku-ku
Tokyo 162-8666
Japan

E-mail: tokano@abmes.twmu.ac.jp

Received: July 6, 2009
Accepted: September 28, 2009
Online Publication Date: November 9, 2009

Biochemical and Biophysical Research Communications 389 (2009) 274–278

Contents lists available at ScienceDirect

Biochemical and Biophysical Research Communications

journal homepage: www.elsevier.com/locate/ybbrc

Nectin-3 expression is elevated in limbal epithelial side population cells with strongly expressed stem cell markers

Risa Kusanagi [a,b], Terumasa Umemoto [a], Masayuki Yamato [a,*], Yu Matsuzaki [a,c], Kohji Nishida [d], Yoshiro Kobayashi [c], Fumio Fukai [b], Teruo Okano [a]

[a] Institute of Advanced Biomedical Engineering and Science, Tokyo Women's Medical University, 8-1 Kawada-cho, Shinjuku-ku, Tokyo 162-8666, Japan
[b] Department of Molecular Patho-Physiology, Tokyo University of Science, 2641 Yamazaki, Noda-Shi, Chiba 278-8510, Japan
[c] Department of Biomolecular Science, Toho University, 3-3-1 Miyama, Funabashi-shi, Chiba 274-8510, Japan
[d] Department of Ophthalmology and Visual Science, Tohoku University Graduate School of Medicine, 1-1 Seiryo-machi, Aoba-ku, Sendai, Miyagi 980-8574, Japan

ARTICLE INFO

Article history:
Received 17 August 2009
Available online 28 August 2009

Keywords:
Corneal epithelium
Limbal epithelium
Stem cell
Side population
Nectin-3
CD61

ABSTRACT

Corneal epithelial stem cells (CESCs) are essential for maintaining the ocular surface. However, the lack of surface markers for CESCs remains a serious obstacle in the identification of CESCs. Previously, we showed that rabbit limbal epithelial side population (rLE-SP) cells exhibited stem cell phenotypes including increased expression of CD61, a marker for mouse hematopoietic stem cells. Here, we demonstrate that nectin-3, an immunoglobulin-like cell–cell adhesion molecule, is highly expressed in rLE-SP cells. Additionally, nectin-3$^+$ cells were significantly enriched among CD61$^+$rLE-SP cells as compared to CD61$^-$rLE-SP cells. In mouse bone marrow side population cells, a correlation between expression of nectin-3 and CD61 was also observed. These data strongly suggest that nectin-3 may contribute to the identification of CESCs.

Introduction

In stem cell biology, the identification of markers that distinguish stem cells from their differentiated progeny is essential for a clear understanding of stem cell properties. In the corneal epithelial system, stem cells are thought to reside in the basal layer of the limbal epithelium [1–3], a transitional zone between the cornea and the peripheral bulbar conjunctiva. Corneal epithelial stem cells (CESCs) maintain the ocular surface by generating transient amplifying cells that migrate, proliferate and differentiate to replace lost or damaged corneal epithelial cells [3–5]. However, the lack of definitive surface markers remains a serious obstacle to the unequivocal identification of CESCs. Although colony-forming assays and pulse-chase experiments with labeled thymidine are traditionally used to identify epithelial stem cells, these cannot accurately assess their function.

We previously demonstrated that the rabbit limbal epithelium contains side population (SP) cells with stem cell-like phenotypes including maintenance of quiescent state, which is unlike previously defined epithelial stem cells that showed high proliferation ability *in vitro* under the culture conditions for epithelial cells [6]. This strongly suggested that rabbit limbal epithelial SP (rLE-SP) cells might allow for new insights into epithelial stem cell populations. Moreover, we recently found that high expression of CD61 was commonly observed in SP cells derived from either mouse bone marrow or rabbit limbal epithelium, and we demonstrated that the CD61^{High} population exhibited superior ability for long-term repopulation in mouse bone marrow SP (mBM-SP) cells or CD34$^-$/c-kit$^+$/Sca-1$^+$/Lineage$^-$ (CD34$^-$KSL) cells, which is regarded as one of the most enriched HSC populations [7,8]. Recently, nectin-3, an emerging immunoglobulin (Ig)-like cell–cell adhesion molecule at adherence junctions (AJs), was reported to play pivotal roles in the cross-talk between cell–matrix and cell–cell junctions as well as the formation of cadherin-based AJs by cooperating with CD51/CD61 (integrin $\alpha_V\beta_3$) signals [9].

In the present study, we found that nectin-3 was highly expressed in rLE-SP cells exhibiting high expression of stem cell markers, suggesting that nectin-3 might be a marker of CESCs.

Materials and methods

Cell preparation. Cell suspensions of rabbit limbal epithelial cells and mouse bone marrow were prepared from New Zealand white

Abbreviations: CESC, corneal epithelial stem cell; HSC, hematopoietic stem cell; CD34$^-$KSL, CD34$^-$/c-kit$^+$/Sca-1$^+$/Lineage$^-$; SP, side population; rLE-SP, rabbit limbal epithelial side population; mBM-SP, mouse bone marrow side population; TPS-A, tryprostatin-A; NSP, non-side population; ABCG2, ATP binding cassette transporter G2; jam-b, junction adherence molecule-b; GAPDH, glyceraldehyde-3-phosphate dehydrogenase.

* Corresponding author. Fax: +81 3 3358 7428.
E-mail address: myamato@abmes.twmu.ac.jp (M. Yamato).

0006-291X/$ - see front matter © 2009 Elsevier Inc. All rights reserved.
doi:10.1016/j.bbrc.2009.08.130

rabbits and C57BL/6 mice, respectively, as described previously [6,10].

Hoechst 33342 exclusion assay using fluorescence activated cell sorting (FACS). Analysis and sorting of SP cells were performed as described previously [6,10]. Briefly, isolated rabbit limbal epithelial cells or mouse bone marrow Lineage$^-$ cells obtained by magnetic cell sorting (Auto MACS system, Miltenyi Biotec, Inc., Bergisch Gladbach, Germany) were stained with 5 μg/ml Hoechst 33342 (Sigma, St. Louis, MO) for 90 min at 37 °C. For inhibition experiments, 50 μM of tryprostatin-A (Alexis Biochemicals, Carlsbad, CA) was added to the staining medium 30 min before the addition of Hoechst 33342. Analysis and cell sorting were then performed using an EPICS® ALTRA FACS analysis system (Beckman Coulter, Fullerton, CA).

Gene expression analysis. Gene expression analysis was performed as described previously [6,10]. Briefly, total RNA was obtained from 10,000 cells of each population using Isogen (Nippongene, Tokyo, Japan), followed by synthesis of single stranded cDNA with the Superscript First-strand System III for RT-PCR (Invitrogen, Carlsbad, CA). Primer pairs and TaqMan® MGB probes were designed for the indicated genes with the TaqMan® gene expression assay™ (Applied Biosystems, Foster City, CA). Quantitative PCR was performed with a 7300 Real Time PCR System (Applied Biosystems). mRNA expression levels were normalized with the expression level of GAPDH.

Immunofluorescence analysis. Cells isolated by FACS were fixed with 4% paraformaldehyde, followed by permeabilization with 0.2% Triton X-100. After incubation with 5% bovine serum albumin (Sigma) to block nonspecific reactions, cells were incubated with anti-nectin-3 antibody (H-245, Santa Cruz Biotechnology, Inc., Santa Cruz, CA) and anti-CD61 antibody (C-20, Santa Cruz Biotechnology, Inc.) for 1 h at room temperature and washed three times with Dulbecco's phosphate buffer saline (PBS). Cells incubated identically with normal rabbit and goat IgG were used as negative controls. After incubation with Alexa Fluor® 546-conjugated anti rabbit IgG antibody (Molecular Probes, Eugene, OR) and Alexa Fluor® 488-conjugated anti goat IgG antibodies (Molecular Probes) for 1 h at room temperature, cells were again washed three times with PBS. Stained cells were finally counter-stained with 10 μg/ml Hoechst 33258 to visualize cell nuclei and observed using confocal laser scanning microscopy (LSM510 Laser Scanning Microscope, Carl ZIEEZ, Germany).

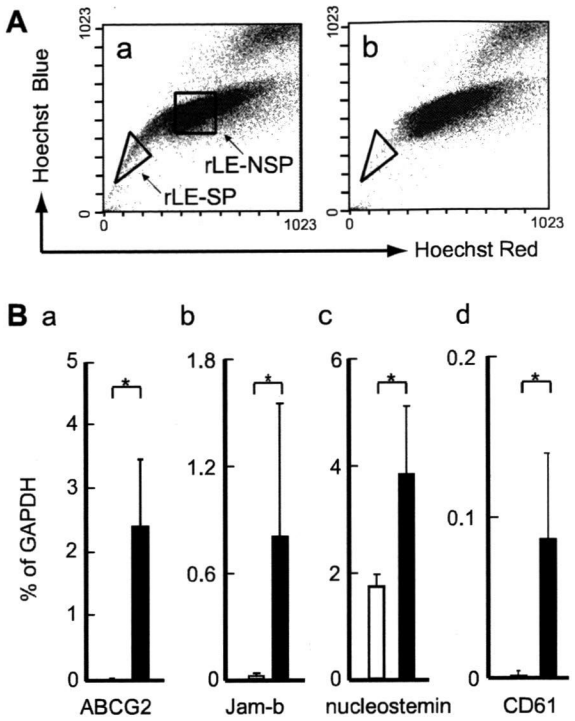

Fig. 1. Rabbit limbal epithelial SP (rLE-SP) cells strongly express stem cell markers. Epithelial cells were removed from the limbus and analyzed for Hoechst 33342 efflux by FACS. SP cells were detected in limbal epithelial cells after Hoechst 33342 staining (A). In the dot plot of (a), the cells denoted by each enclosed area were regarded as rLE-SP cells or rLE-NSP cells for further characterization. Limbal epithelial cells were pre-treated with tryprostatin-A (TPS-A), a specific inhibitor of ABCG2 (b), prior to staining with Hoechst 33342. Using isolated rLE-SP cells and rLE-NSP cells, expression of stem cell markers was examined with real-time quantitative PCR (B). Relative expression of the selected genes was normalized to that of GAPDH for each sample. mRNA expression of ABCG2 (a), jam-b (b), nucleostemin (c), and CD61 (d) are shown. Expression levels were determined from rLE-SP cells: black bars, and rLE-NSP cells: white bars, for each individual mRNA. Data represent the mean value from four to six samples. Error bars indicate the SD (*$p < 0.05$).

Results

Rabbit limbal epithelial cells were subjected to a Hoechst 33342 dye efflux assay that detected a distinct SP cell population with reduced Hoechst 33342 blue/red fluorescence (Fig. 1A; 0.40% gated cells). Treatment with tryprostatin-A (TPS-A), a specific inhibitor of a mediator of the SP phenotype (ATP binding cassette transporter G2, or ABCG2), eliminated this population (Fig. 1B). Moreover, much higher expression of ABCG2 was observed in rLE-SP cells than in non-SP (NSP) cells. In addition, compared to NSP cells, rLE-SP cells showed higher expression of stem cell markers such as jam-b (junction adherence molecule-b), which is highly expressed in several stem cells [11]; nucleostemin, which controls the cell cycle and maintenance capacities of various stem cells [12–14]; and CD61 (Fig. 1B). These results strongly supported the idea that rLE-SP cells are enriched with CESCs.

To identify candidate CESC markers, we focused on six surface molecules (MMP-14, CD47, CD36, nectin-1, nectin-3, and necl-5) that were reported to be associated with CD61. MMP-14, also known as MT1-MMP, was reported to activate MMP-2 by cooperating with CD51/CD61 [15,16]. CD47, also known as integrin-associated protein (IAP), is physically and functionally associated with CD61 (CD51/CD61) and involved in the increase in intracellular calcium concentration that occurs upon endothelial cell adhesion to the extracellular matrix [17]. CD36, also known as thrombospondin receptor/scavenger receptor, was also reported to associate with CD61 [18]. Nectin-1, nectin-3, and necl-5, members of the nectin/necl family, were reported to regulate cell functions such as migration, proliferation and AJ formation by cooperating with CD51/CD61 [19].

Quantitation of the expression of these genes in rLE-SP cells using real-time quantitative RT-PCR revealed that nectin-3 and necl-5 are more highly expressed in rLE-SP cells than in NSP cells (Fig. 2e and f). In contrast, differential expression of nectin-1 and CD47 was not observed between rLE-SP cells and NSP cells (Fig. 2b and d), and neither CD36 nor MMP-14 expression was detected in any of the fractions (Fig. 2a and c). Therefore, these results suggest that the expression of nectin-3 and necl-5 is specifically enhanced in CESCs.

Since SP phenotype is accepted as a common property of somatic stem cells, we speculated that the expression pattern of genes concerned with characters of somatic stem cells may be conserved among SP cells isolated from various tissues. Therefore, further screening was performed by gene expression assays for molecules highly expressed in rLE-SP cells using mBM-SP cells, which were regarded as a population of quiescent HSCs. When

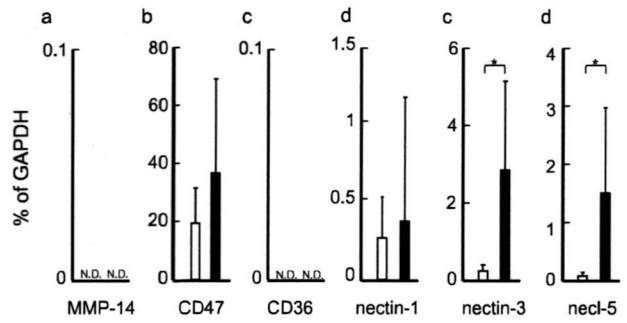

Fig. 2. Expression of CD61-associated molecules in rLE-SP cells. Using total RNA derived from rLE-SP cells and rLE-NSP cells, expression of the indicated CD61-associated molecules was investigated by real-time quantitative PCR. Relative expression of the selected genes was normalized to that of GAPDH for each sample. mRNA expression of MMP-14 (a), CD47 (b), CD36 (c), nectin-1 (d), nectin-3 (e), and necl-5 (f) are shown. Expression levels were determined from rLE-SP cells: black bars, and rLE-NSP cells: white bars, for each individual mRNA. Data represent the mean value from four to six samples. Error bars indicate the SD (*$p < 0.05$).

the expression of nectin-3 and necl-5 was examined in mouse bone marrow, only nectin-3 showed significantly higher expression in SP cells compared to NSP cells (Fig. 3). Therefore, we focused on nectin-3 as a candidate CESC marker.

Since the gene expression analysis showed that higher mRNA expression of nectin-3 was observed in rLE-SP cells, rLE-SP cells were subjected to immunofluorescent staining to confirm expression of nectin-3 at the protein level. Analysis with a confocal laser microscope revealed that a portion of rLE-SP cells expressed nectin-3 (Fig. 4A). Additionally, the frequency of nectin-3$^+$ cells was higher in rLE-SP cells than in NSP cells (Fig. 4A). In mouse bone marrow, the relationship between nectin-3$^+$ cells and SP cells was similar to that in rabbit limbal epithelium (Fig. 4A).

Previously, we demonstrated that CD61^{High} fractions significantly contained more HSCs than CD61^{Low} fractions in SP and CD34$^-$KSL cells [7,8]. Therefore, we examined the expression of nectin-3 in a CD61^{High} population of rLE-SP cells, since rLE-SP cells also display enhanced CD61mRNA levels (Fig. 1). When limbal epithelial cells were stained with anti-CD61 antibody, the frequency of CD61$^+$ cells was also higher in rLE-SP cells than in NSP cells (data not shown). Moreover, the majority of the CD61$^+$ fraction in rLE-SP cells showed expression of nectin-3 (Fig. 4A and B). In contrast, the CD61$^-$ fraction in rLE-SP cells contained hardly any nectin-3$^+$ cells (Fig. 4A). In mBM-SP cells, nectin-3$^+$ cells were also enriched in the CD61$^+$ fraction, but not in the CD61$^-$ fraction (Fig. 4A and B). Thus, these results strongly support the idea that CESCs preferentially express nectin-3.

Discussion

Herein, we demonstrated that nectin-3 is highly expressed in both rLE-SP cells (Fig. 2) and mBM-SP cells (Fig. 3). Moreover, further enhanced expression of nectin-3 was observed in CD61$^+$ fractions of rLE-SP and mBM-SP cells (Fig. 4). Therefore, these results indicate that CESCs exhibit high expression of nectin-3. However, it seems that expression of nectin-3 is not a completely specific phenotype for CESCs, since a small portion of NSP cells (the percentage is low but not dismissible) showed expression of nectin-3 in limbal epithelium (Fig. 4). Therefore, combination with another stem cell marker (such as the SP phenotype (ABCG2)) is essential for high-grade identification and isolation of CESCs.

Unlike generally accepted epithelial stem cells that display high proliferative potential *in vitro*, rLE-SP cells exhibited no proliferative capability *in vitro* under normal culture conditions for epithelial cells [6]. However, rLE-SP cells had stem cell-like properties, including growth arrest in the quiescent state [6], thus meeting the criteria of other adult stem cells [20]. To accurately identify epithelial stem cells, it seems important to meet the criteria shared with various adult stem cells such as HSCs that are regarded to generally reside in the quiescent state [20]. We previously focused on CD61 by comparison between SP cells derived from rabbit limbal epithelium versus mouse bone marrow [7]. In the present study, the possibility that CESCs highly express nectin-3 was raised from the genes whose expression is commonly increased in these SP cells. Thus, comparisons between SP fractions derived from different tissues seem likely to contribute to screening for a marker of somatic stem cells.

The nectin family is associated with afadin via its intracellular domain, which regulates many biological events such as cell adhesion, polarity, proliferation and migration by modulating outside-in signals via integrin family and cytokine receptors [9,19,21]. Actually, nectin-3 was reported to cis-interact with CD51/CD61 at nectin-based cell–cell adhesion sites, and activation of CD51/CD61 was controlled by nectin signaling in response to the condition of AJs [9]. Previously, we suggested that CD61 was involved in HSC function due to the correlation between expression of CD61 and the ability for long-term repopulation [7,8]. In the present study, we showed that the majority of CD61$^+$ rLE-SP cells express nectin-3, and these molecules co-localize on the plasma membrane

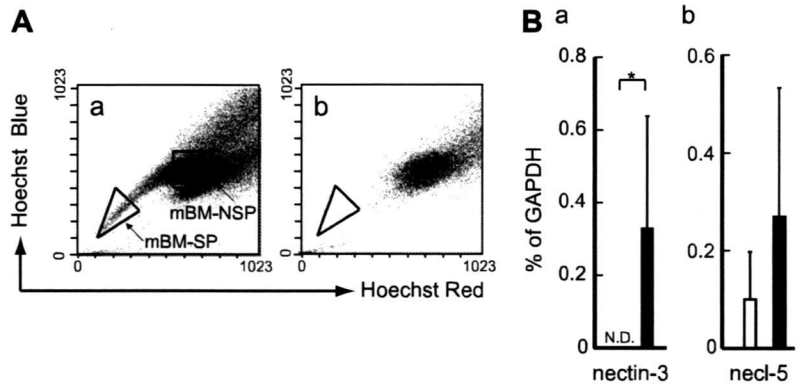

Fig. 3. Expression of CD61-associated molecules in mouse bone marrow SP (mBM-SP) cells. Mouse bone marrow Lineage$^-$ cells obtained by MACS were stained with Hoechst 33342 (A) and sorted into SP and NSP cells, respectively (a). Lineage$^-$ cells were pre-treated with tryprostatin-A (TPS-A), a specific inhibitor of ABCG2 (b), prior to staining with Hoechst 33342. After isolation, total RNA extracted from mBM-SP cells and mBM-NSP cells was subjected to real-time quantitative PCR (B). The expression of the selected genes was normalized to that of GAPDH for each sample. mRNA levels of nectin-3 (a) and necl-5 (b) are shown. Expression levels were determined from mBM-SP cells: black bars, and mBM-NSP cells: white bars, for each individual mRNA. Data represent the mean value from four to six samples. Error bars indicate the SD (*$p < 0.05$).

A

	Rabbit limbal epithelium	Mouse bone marrow
NSP	0.78 (8/1349)	2.28 (11/482)
SP	3.20 (46/1436)	8.05 (38/472)
$CD61^-$ SP	0.72 (10/1381)	1.16 (5/430)
$CD61^+$ SP	65.5 (36/55)	78.6 (33/42)

% of nectin-3^+ cells

B

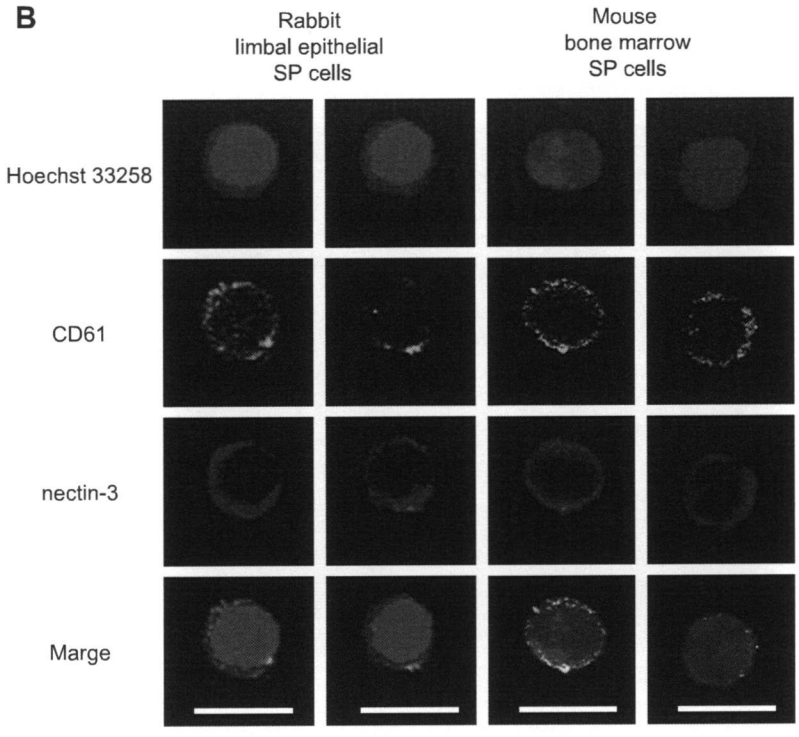

Fig. 4. Nectin-3 positive cells were observed in SP cells. Immunofluorescence analysis was performed using SP cells derived from both limbal epithelium and mouse bone marrow. The table presents the percentage of nectin-3^+ cells in each indicated fraction (A). Nectin-3^+ cells and total cells are indicated by the numbers in parentheses. The panels represent $CD61^+$SP cells with expression of nectin-3, which were stained with Hoechst (blue), anti-CD61 antibody (green) and anti-nectin-3 antibody (red). Scale bars represent 10 μm.

(Fig. 4B). Thus, these data suggest that cross-talk between outside-in signals via CD61 and nectin-3 may be involved in the control of CESCs.

In addition, trans-interactions of nectin-3 with itself were also reported to recruit the cadherin family following the establishment of AJs [20]. Recently, some reports suggested that N-cadherin was involved in the somatic stem cell niche. N-cadherin$^+$ cells residing in limbal epithelium were reported to show high expression of stem cell markers and colony-forming efficiency [22]. Moreover, HSCs contacted osteoblasts (an HSC niche cell candidate) via N-cadherin [20,23]. Thus, these results suggest that nectin-3 may also be involved in cadherin-based AJs in tissue-specific stem cells.

By contrast, in addition to the genes (ABCG2, Bmi-1, and nestin) previously reported by us [6], the present study demonstrated that rLE-SP cells show high expression of the stem cell markers jam-b, nucleostemin, and CD61. jam-b is an Ig-like protein consisting of two extracellular Ig domains, a short cytoplasmic tail and a PDZ-domain-binding motif. Expression of jam-b was reported to be commonly observed in embryonic stem cells, HSCs and neural stem cells, but not in their differentiated progeny [11]. In limbal epithelium, expression of jam-b was observed in rLE-SP cells but not in NSP cells (Fig. 1B). Thus, the increased expression of jam-b in SP cells also seems likely to contribute to distinguishing CESCs from their differentiated progeny in limbal epithelium.

Nucleostemin is a nucleolar protein detected in embryonic stem cells, adult central neural system (CNS) stem cells, primitive cells in the bone marrow and cancer cells [13,14,24]. Moreover, nucleostemin has been suggested to play a role in controlling cell-cycle progression in several stem cells and cancer cells [14,25]. Recently, it was reported that high expression of nucleostemin was essential for the maintenance of capacities in germline stem cells [12]. In limbal epithelium, expression of nucleostamin was enhanced in rLE-SP cells compared to NSP cells (Fig. 1B). Therefore, increased nucleostamin expression may also be involved in the maintenance of stem-ness in CESCs.

CD61, also known as integrin β_3 or GPIIIb, functions as a receptor for the extracellular matrix by heterodimerization with a proper integrin α subunit. Previously, CD61 was reported to be commonly expressed in rLE-SP cells and mBM-SP cells [7]. Moreover, the present study demonstrated that rLE-SP cells showed higher expression of CD61 mRNA (Fig. 1B) and were confirmed to contain $CD61^+$ cells (Fig. 4A). Moreover, the frequency of $CD61^+$ cells was higher in rLE-SP cells than in NSP cells (data not shown). Although it was generally known that differentiated epithelial cells barely expressed

CD61, it was reported that mammary gland epithelial cancer stem cells showed high expression of CD61 [26]. In addition, the $CD61^{High}$ fraction exhibited a higher capacity for long-term repopulation than the $CD61^{Low}$ fraction in mBM-SP cells [7]. Therefore, these results strongly suggest that the extraction of the $CD61^{High}$ fraction from the rLE-SP fraction also contributes to greater enrichment for CESCs. Thus, the increased expression of these stem cell markers in rLE-SP cells strongly supports the idea that CESCs that reside in the quiescent state are enriched in rLE-SP cells, and it suggests that jam-b, nucleostemin, and CD61 can also be used as markers of CESCs.

However, unlike the hematopoietic system where there is an established and accepted *in vivo* reconstitution assay, an analogous model for the corneal epithelial system is currently lacking. This is a serious obstacle to the accurate assessment of CESC functions such as self-renewal and long-term maintenance. In addition, due to the lack of a commercially available antibody against rabbit nectin-3, we have not been able to show that CESCs can be isolated by expression of nectin-3. However, the analyses of stem cell marker expression more strongly support the idea that CESCs are concentrated among rLE-SP cells (Fig. 1B), and the increased expression of nectin-3 in the majority of $CD61^{+}$ rLE-SP cells suggests that CESCs express nectin-3 (Fig. 4).

In conclusion, our findings indicate that CESCs strongly express nectin-3, and this may contribute to the identification and isolation of CESCs as well as to the determination of stem-ness properties of CESCs such as niche interactions and quiescence.

Acknowledgments

This study was partially supported by Formation of Innovation Center for Fusion of Advanced Technologies in the Special Coordination Funds for Promoting Science and Technology "Cell Sheet Tissue Engineering Center (CSTEC)" from the Ministry of Education, Culture, Sports, Science and Technology (MEXT), Japan.

References

[1] G. Cotsarelis, S.Z. Cheng, G. Dong, T.T. Sun, R.M. Lavker, Existence of slow-cycling limbal epithelial basal cells that can be preferentially stimulated to proliferate: implications on epithelial stem cells, Cell 57 (1989) 201–209.
[2] A. Schermer, S. Galvin, T.T. Sun, Differentiation-related expression of a major 64K corneal keratin in vivo and in culture suggests limbal location of corneal epithelial stem cells, J. Cell Biol. 103 (1986) 49–62.
[3] R.A. Thoft, J. Friend, Biochemical transformation of regenerating ocular surface epithelium, Invest. Ophthalmol. Vis. Sci. 16 (1977) 14–20.
[4] R.C. Buck, Measurement of centripetal migration of normal corneal epithelial cells in the mouse, Invest. Ophthalmol. Vis. Sci. 26 (1985) 1296–1299.
[5] S. Kinoshita, J. Friend, R.A. Thoft, Sex chromatin of donor corneal epithelium in rabbits, Invest. Ophthalmol. Vis. Sci. 21 (1981) 434–441.
[6] T. Umemoto, M. Yamato, K. Nishida, J. Yang, Y. Tano, T. Okano, Limbal epithelial side-population cells have stem cell-like properties, including quiescent state, Stem Cells 24 (2006) 86–94.
[7] T. Umemoto, M. Yamato, Y. Shiratsuchi, M. Terasawa, J. Yang, K. Nishida, Y. Kobayashi, T. Okano, Expression of Integrin beta3 is correlated to the properties of quiescent hemopoietic stem cells possessing the side population phenotype, J. Immunol. 177 (2006) 7733–7739.
[8] T. Umemoto, M. Yamato, Y. Shiratsuchi, M. Terasawa, J. Yang, K. Nishida, Y. Kobayashi, T. Okano, CD61 enriches long-term repopulating hematopoietic stem cells, Biochem. Biophys. Res. Commun. 365 (2008) 176–182.
[9] Y. Sakamoto, H. Ogita, T. Hirota, T. Kawakatsu, T. Fukuyama, M. Yasumi, N. Kanzaki, M. Ozaki, Y. Takai, Interaction of integrin alpha(v)beta3 with nectin. Implication in cross-talk between cell–matrix and cell–cell junctions, J. Biol. Chem. 281 (2006) 19631–19644.
[10] T. Umemoto, M. Yamato, K. Nishida, J. Yang, Y. Tano, T. Okano, p57Kip2 is expressed in quiescent mouse bone marrow side population cells, Biochem. Biophys. Res. Commun. 337 (2005) 14–21.
[11] T. Sakaguchi, M. Nishimoto, S. Miyagi, A. Iwama, Y. Morita, N. Iwamori, H. Nakauchi, H. Kiyonari, M. Muramatsu, A. Okuda, Putative "stemness" gene jam-B is not required for maintenance of stem cell state in embryonic, neural, or hematopoietic stem cells, Mol. Cell. Biol. 26 (2006) 6557–6570.
[12] M. Ohmura, K. Naka, T. Hoshii, T. Muraguchi, H. Shugo, A. Tamase, N. Uema, T. Ooshio, F. Arai, K. Takubo, G. Nagamatsu, I. Hamaguchi, M. Takagi, M. Ishihara, K. Sakurada, H. Miyaji, T. Suda, A. Hirao, Identification of stem cells during prepubertal spermatogenesis via monitoring of nucleostemin promoter activity, Stem Cells 26 (2008) 3237–3246.
[13] R.Y. Tsai, R.D. McKay, A nucleolar mechanism controlling cell proliferation in stem cells and cancer cells, Genes Dev. 16 (2002) 2991–3003.
[14] D. Normile, Cell proliferation. Common control for cancer, stem cells, Science 298 (2002) 1869.
[15] P.C. Brooks, S. Stromblad, L.C. Sanders, T.L. von Schalscha, R.T. Aimes, W.G. Stetler-Stevenson, J.P. Quigley, D.A. Cheresh, Localization of matrix metalloproteinase MMP-2 to the surface of invasive cells by interaction with integrin alpha v beta 3, Cell 85 (1996) 683–693.
[16] R.E. Seftor, E.A. Seftor, W.G. Stetler-Stevenson, M.J. Hendrix, The 72 kDa type IV collagenase is modulated via differential expression of alpha v beta 3 and alpha 5 beta 1 integrins during human melanoma cell invasion, Cancer Res. 53 (1993) 3411–3415.
[17] M.A. Schwartz, E.J. Brown, B. Fazeli, A 50-kDa integrin-associated protein is required for integrin-regulated calcium entry in endothelial cells, J. Biol. Chem. 268 (1993) 19931–19934.
[18] W.M. Miao, E. Vasile, W.S. Lane, J. Lawler, CD36 associates with CD9 and integrins on human blood platelets, Blood 97 (2001) 1689–1696.
[19] Y. Takai, W. Ikeda, H. Ogita, Y. Rikitake, The immunoglobulin-like cell adhesion molecule nectin and its associated protein afadin, Annu. Rev. Cell Dev. Biol. 24 (2008) 309–342.
[20] F. Arai, A. Hirao, M. Ohmura, H. Sato, S. Matsuoka, K. Takubo, K. Ito, G.Y. Koh, T. Suda, Tie2/angiopoietin-1 signaling regulates hematopoietic stem cell quiescence in the bone marrow niche, Cell 118 (2004) 149–161.
[21] N. Kanzaki, H. Ogita, H. Komura, M. Ozaki, Y. Sakamoto, T. Majima, T. Ijuin, T. Takenawa, Y. Takai, Involvement of the nectin-afadin complex in PDGF-induced cell survival, J. Cell Sci. 121 (2008) 2008–2017.
[22] R. Hayashi, M. Yamato, H. Sugiyama, T. Sumide, J. Yang, T. Okano, Y. Tano, K. Nishida, N-Cadherin is expressed by putative stem/progenitor cells and melanocytes in the human limbal epithelial stem cell niche, Stem Cells 25 (2007) 289–296.
[23] J. Zhang, C. Niu, L. Ye, H. Huang, X. He, W.G. Tong, J. Ross, J. Haug, T. Johnson, J.Q. Feng, S. Harris, L.M. Wiedemann, Y. Mishina, L. Li, Identification of the haematopoietic stem cell niche and control of the niche size, Nature 425 (2003) 836–841.
[24] W. Kafienah, S. Mistry, C. Williams, A.P. Hollander, Nucleostemin is a marker of proliferating stromal stem cells in adult human bone marrow, Stem Cells 24 (2006) 1113–1120.
[25] H. Ma, T. Pederson, Nucleostemin: a multiplex regulator of cell-cycle progression, Trends Cell Biol. 18 (2008) 575–579.
[26] F. Vaillant, M.L. Asselin-Labat, M. Shackleton, N.C. Forrest, G.J. Lindeman, J.E. Visvader, The mammary progenitor marker CD61/beta3 integrin identifies cancer stem cells in mouse models of mammary tumorigenesis, Cancer Res. 68 (2008) 7711–7717.

Histological evaluation of mechanical epithelial separation in epithelial laser in situ keratomileusis

Takeshi Soma, MD, Kohji Nishida, MD, PhD, Masayuki Yamato, PhD, Seiichi Kosaka, Joseph Yang, Ryuhei Hayashi, MSc, Hiroaki Sugiyama, MSc, Naoyuki Maeda, MD, PhD, Teruo Okano, PhD, Yasuo Tano, MD, PhD

PURPOSE: To evaluate the effect of mechanical epithelial separation with an epikeratome on the histologic ultrastructure of epithelial flaps and stromal beds from human corneas.

SETTING: Departments of Ophthalmology, Osaka University Medical School, Osaka, and Tohoku University School of Medicine, Sendai, and Institute of Advanced Biomedical Engineering and Science and Medical Research Institute, Tokyo Women's Medical University, Tokyo, Japan.

METHODS: Eye-bank eyes were deepithelialized using an Epi-K epikeratome. Epithelial flaps and stromal beds were assessed by light and electron microscopy. Immunofluorescence staining for types IV and VII collagens, integrins α_6 and β_4, and laminin 5 was also performed.

RESULTS: Four eyes were evaluated. On scanning electron microscopy, the cleavage planes of epithelial flaps and stromal beds were relatively smooth. On transmission electron microscopy, epithelial flaps were separated partially within the lamina fibroreticularis and partially within the lamina lucida. Immunofluorescence showed positive staining for type VII collagen and discontinuous staining for type IV collagen in stromal beds. Discontinuous linear staining for types IV and VII collagens was observed in epithelial flaps. Staining for integrins α_6 and β_4 was positive in some regions and discontinuous in other regions of epithelial flaps. In stromal beds, integrins α_6 and β_4 had a patchy expression pattern. Staining for laminin 5 was intermittently positive along the basal side of epithelial flaps and stromal beds.

CONCLUSIONS: Epithelial flaps created with an epikeratome were mechanically separated partly within the lamina fibroreticularis and partly within the lamina lucida. Stromal beds had relatively smooth surfaces with no obvious trauma to Bowman layer.

J Cataract Refract Surg 2009; 35:1251–1259 © 2009 ASCRS and ESCRS

Laser in situ keratomileusis (LASIK) is currently the most popular technique to surgically correct refractive errors. Compared with photorefractive keratectomy (PRK), LASIK provides several advantages including rapid visual recovery, reduced postoperative pain, and minimal corneal haze.[1,2] However, LASIK complications related to the corneal flap, such as buttonholes, free flaps, flap striae, epithelial ingrowth, and corneal ectasia, can develop postoperatively.[3–5]

In 1999, Camellin introduced laser-assisted subepithelial keratectomy (LASEK), a modification of conventional PRK. With this technique, an epithelial flap is created using a dilute ethanol solution to loosen the epithelial layer (U. Cimberle, "LASEK May Offer the Advantages of Both LASIK and PRK," Ocular Surgery News, March 1, 1999, page 28). After ablation, the epithelial flap is repositioned on the stromal bed. Therefore, LASEK can avoid the flap-related complications observed with LASIK because no stromal flap is created. Researchers report that LASEK is more effective than conventional PRK in the correction of moderate myopia[6,7] and that LASEK is better than LASIK in the uniformity of the corneal topography, corrected visual acuity, and contrast sensitivity 6 months postoperatively.[8] Despite these promising results, there are substantial concerns about the possible toxicity of ethanol to the epithelial flap and the underlying stroma after LASEK.[9,10]

In 2003, Pallikaris et al.[11] introduced the refractive surgical technique of epithelial LASIK (epi-LASIK). In this technique, an epithelial flap is created by mechanical separation using an epikeratome, a device

doi:10.1016/j.jcrs.2009.02.025

similar to a microkeratome. After mechanical separation and photoablation on the underlying stromal bed, the epithelial flap is replaced on the stroma, similar to the LASEK method. Because epi-LASIK procedures do not require alcohol or other chemical agents to create an epithelial flap, researchers have theorized that mechanical separation can avoid the toxic effects of alcohol on the epithelial flap and stromal bed and provide an automated surgical procedure with a short learning curve for LASIK surgeons.[12]

During mechanical separation in epi-LASIK procedures, the points of anchoring between the corneal epithelium and stroma are cleaved. At these positions, hemidesmosomes normally connect the basal epithelial cells to the basement membrane. Within the hemidesmosomes of basal corneal epithelial cells, the transmembrane proteins integrin α_6 and integrin β_4 adhere to laminin 5, which is a major basement membrane component.[13,14] The basement membrane comprises 3 layers: the lamina lucida, the lamina densa, and the lamina fibroreticularis. The lamina densa is a sheet-like structure made up of the extracellular matrix (ECM) molecules type IV collagen, laminin, entactin–nidogen, and perlecan. The lamina fibroreticularis lies beneath the lamina densa, contains anchoring fibrils comprising type VII collagen, and forms a complex network with type I and type V collagens to attach the epithelium and its basement membrane to the underlying Bowman layer (Figure 1).[15–17]

Although the clinical outcomes of epi-LASIK have been evaluated,[18–20] the exact site of epithelial separation during epi-LASIK remains unclear. Pallikaris et al.[12] found that the epithelial separation was beneath the basement membrane with intact basal cells. Kollias et al.[21] found that the basal cell layer of the epithelial flap had normal morphology with interruptions of the basement membrane. However, Tanioka et al.[22] report that the basement membrane was lost and the basal cells were damaged in some regions. In addition, a detailed study of the cleavage planes in the epithelial flap and stromal bed in epi-LASIK has not been performed.

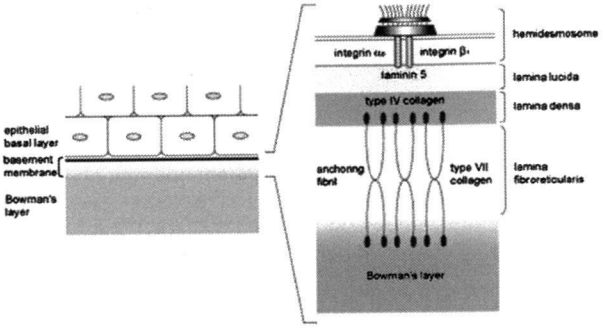

Figure 1. Schematic diagram of epithelial anchorage to the stroma. (Distances and sizes are not to scale.)

In the current study, we evaluated the cleavage plane of the epithelial flap mechanically separated with an epikeratome and the underlying stromal bed in epi-LASIK. We also identified details of the exact site of cleavage in the epithelial flap after mechanical separation.

MATERIALS AND METHODS

This study adhered to the tenets of Declaration of Helsinki regarding the use of human tissue specimens.

Mechanical Separation

Intact human donor eyes (Northwest Lions Eye Bank) were obtained 5 hours 16 minutes to 5 hours 28 minutes after donor death and stored in a conventional moist chamber for 3 to 6 days at 4°C. Epithelial separation was performed using the Epi-K epikeratome (Moria). This device has a disposable oscillating head (oscillation rate 15 000 rpm) encasing a preassembled noncutting stainless-steel blade to mechanically separate the epithelial layer from the underlying stroma using 3 speeds (low, 0.05 mm/s; medium, 0.25 mm/sec; normal, 0.50 mm/s). The assembled head, handpiece, and suction ring were placed on the eye, and suction was activated. After adequate suction (≥65 mm Hg) was confirmed by Barraquer tonometry and a stable reading of lower pressure on the epikeratome console was obtained, the oscillating head was advanced to the horizontal corneal plane at low speed. When the epithelial flap rose and was visible between the separator and the applanation plate, the device was shifted to medium speed, cleaving the epithelial layer. Just after the edge of the separator reached the center of the suction ring, the epithelial flap was cleaved at top speed. When the head reached the stopping point, the footpedal was released and low vacuum was activated. After a stable

Submitted: October 17, 2008.
Final revision submitted: February 13, 2009.
Accepted: February 19, 2009.

From the Departments of Ophthalmology, Osaka University Medical School (Soma, Sugiyama, Maeda, Tano), Osaka, and Tohoku University School of Medicine (Nishida, Hayashi), Sendai, and the Institute of Advanced Biomedical Engineering and Science (Yamato, Yang, Okano) and Medical Research Institute (Kosaka), Tokyo Women's Medical University, Tokyo, Japan.

No author has a financial or proprietary interest in any material or method mentioned.

Supported in part by the High-Tech Research Center Program and the Center of Excellence Program for the 21st Century from the Ministry of Education, Culture, Sports, Science, and Technology, Japan.

Corresponding author: Kohji Nishida, MD, PhD, Department of Ophthalmology, Tohoku University School of Medicine, 1-1 Seiryo-machi, Aoba-ku, Sendai, 980-8574, Japan. E-mail: knishida@oph.med.tohoku.ac.jp.

low-vacuum level was confirmed, the head was moved backward and the device was removed from the eye.

Tissue Processing

Immediately after epithelial separation, the epithelial flaps were excised along the hinge and trisected. The stromal beds were also excised from the globe and trisected. One of each of the specimens was placed in neutral buffered formalin 10% (Nacalai Tesque) and routinely processed for conventional histologic examination. Another specimen from each tissue was immersed in glutaraldehyde 2.0% (Nacalai Tesque) in 0.1 M phosphate buffer (pH 7.4) for scanning electron microscopy (SEM) and transmission electron microscopy (TEM). The third group of specimens was frozen in OTC compound (Tissue-Tec, Sakura Finite) for processing into frozen sections and subsequent immunofluorescence staining.

Histological Analysis

Formalin-fixed specimens were dehydrated with a graded series of ethanol, washed with xylene solution, and processed into 3 μm thick paraffin-embedded sections. Conventional hematoxylin–eosin staining was then performed, and the sections were visualized by light microscopy (BX50, Olympus).

Scanning Electron Microscopy

Glutaraldehyde-fixed specimens were rinsed in phosphate buffer and postfixed in osmium tetroxide 2% for 2 hours at 4°C. The specimens were then dehydrated through a graded series of ethanol and 3-methylbutyl acetate before critical-point drying. The samples were mounted on aluminum stubs, coated with an osmium plasma coater, and examined by SEM (S-4300, Hitachi High-Tech). Cleavage surfaces of the epithelial flaps and stromal beds were examined at 4 magnifications (×20, ×50, ×1000, ×10000).

Transmission Electron Microscopy

Glutaraldehyde-fixed specimens were rinsed in phosphate buffer and postfixed in osmium tetroxide 2% for 2 hours at 4°C. The specimens were dehydrated through a graded series of ethanol and methyl glycidyl ether and embedded in epoxy resin according to standard techniques. Semi-thin sections (5 μm) were then stained with toluidine blue, and a suitable area was chosen. The blocks were trimmed and thin-sectioned (100 nm), stained with uranyl acetate-Reynold lead nitrate 4%, and examined by TEM (H-7100 or H-7650, Hitachi High-Tech).

Immunofluorescence

Frozen specimens were cut into 10 μm-thick sections using a cryostat (Jung CM3000, Leica) at −20°C, mounted on glass slides coated with magnesium aluminosilicate glass, air dried, and stored at −80°C. Sections were incubated with a 1:20 dilution of polyclonal goat anticollagen IV (1340-01, Southern Biotechnology Associates), a 1:1000 dilution of monoclonal mouse anticollagen VII (LH 7.2, Sigma), a 1:100 dilution of monoclonal mouse antiintegrin α_6 (4F10, Chemicon International), a 1:200 dilution of monoclonal mouse antiintegrin β_4 (ASC-8, Chemicon International), or a 1:200 dilution of monoclonal mouse antilaminin 5 (P3H9-2, R&D Systems) overnight at 4°C. The sections were then incubated with fluorescein isothiocyanate–conjugated mouse anti-goat immunoglobulin G (IgG) or goat anti-mouse IgG (both Jackson ImmunoResearch Laboratories) for 2 hours at room temperature. The stained sections were counterstained with Hoechst 33342 for 10 minutes at room temperature to visualize the cell nuclei. Sections incubated identically with equal concentrations of normal mouse and goat Ig or a secondary antibody alone served as negative controls. All sections were viewed by confocal laser scanning microscopy (Fluoview FV1000, Olympus).

RESULTS

Four eye-bank eyes were used in the study.

Epithelial Flaps

Light microscopic examination of the epithelial flap showed that normal stratification and cell morphology were well preserved in all 4 eyes after mechanical separation using the epikeratome. No obvious trauma or blebs were observed in the basal cells of the epithelial flap (Figure 2).

Scanning electron microscopy of the epithelial flaps at low magnification (×50) showed that the bottom surface of the epithelial flap had a relatively smooth surface with little debris (Figure 3, *A*). At a magnification of ×1000, the underside of the epithelial flaps had regions of 2 differing thicknesses in all eyes (Figure 3, *B*). In the thinner regions, the basement membrane appeared to be mostly absent from the epithelial flap (Figure 3, *B*). In contrast, in the thicker regions, the basement membrane seemed to be present on the posterior surface of the epithelial flap (Figure 3, *B*). Overall, in all eyes the thin regions were mainly in the center of the epithelial sheets, resembling spot-like formations, while the thick regions were in the surrounding areas. At higher magnification (×10000), columnar structures and several depressions were seen in the areas of the epithelial flaps without a basement membrane (Figure 3, *C*). However, in the thick regions, the posterior surface of the basement membrane was relatively rough with numerous protuberances

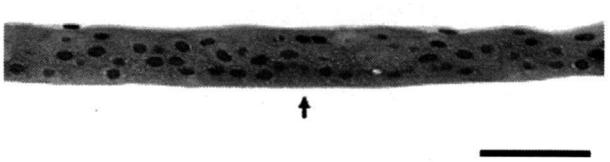

Figure 2. Light micrograph of an epithelial flap after mechanical separation. The arrow indicates the basal side of the epithelial sheet (*bar* = 50 μm).

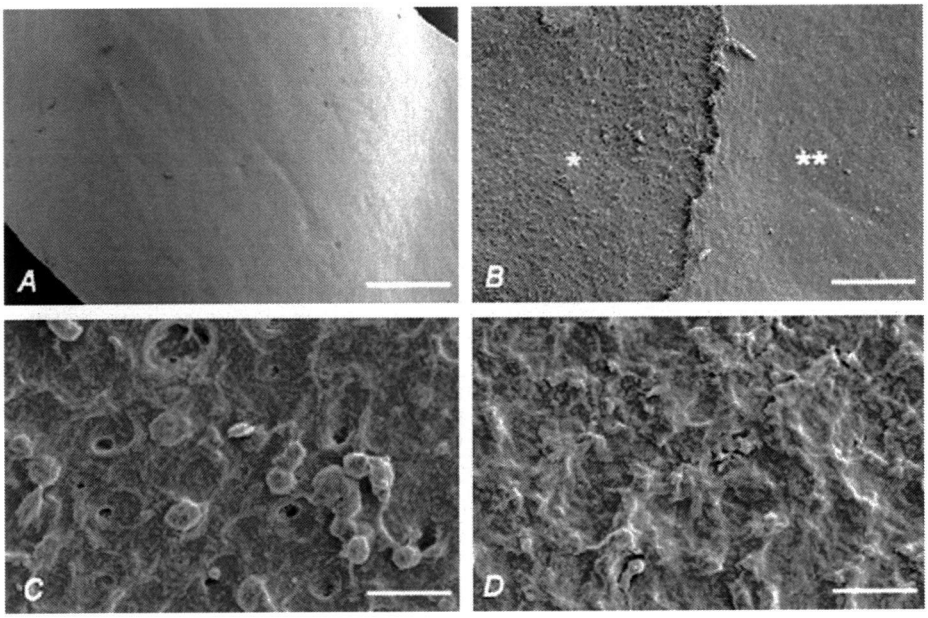

Figure 3. *A*: Scanning electron microscopy of an epithelial flap after mechanical separation at low magnification (×50) (*bar* = 200 µm). *B*: Higher magnification (×1000) view of the panel *A* shows a flap with no basement membrane in the thin regions (*single asterisk*) and a basement membrane on the basal side of the flap in the thick regions (*double asterisk*) (*bar* = 20 µm). *C*: High magnification (×10000) of the thin region of panel *B* shows columnar structures and some depressions on the posterior surface of the epithelial flap (*bar* = 2 µm). *D*: Higher magnification (×10000) of the thick region in panel *B* shows several crest-like protuberances on the underside of the epithelial flap (*bar* = 2 µm).

(Figure 3, *D*). No obviously disrupted basal cells were seen in any cleavage plane in the 4 eyes.

Transmission electron microscopy showed that the epithelial flaps had 2 cleavage planes in all eyes. The first plane was along the lamina lucida (Figure 4, *A*), and the second plane was within the lamina fibroreticularis (Figure 4, *B*). In regions of the epithelial flap where there was no basement membrane, the basal epithelial cells had fewer hemidesmosomes and several small blebs were observed (Figure 4, *A*). In these areas, the plasma membrane on the basal side of the epithelial cells was also occasionally disrupted. Light microscopy and SEM showed no obvious disruption of the basal cells. Hemidesmosome attachments were also cleaved with the lamina lucida.

In contrast, in other regions the epithelial flap was cleaved along with the entire lamina lucida, the intact lamina densa, and a portion of lamina fibroreticularis (Figure 4, *B*). Transmission electron microscopy showed that the basal epithelial cells and their intracellular contacts had normal morphology and that the anchoring of the hemidesmosomes to the basement membrane remained intact. In these regions, the epithelial flap was separated from the underlying stromal bed along with a portion of the basement membrane into the lamina fibroreticularis.

Immunostaining results showed discontinuous linear staining of type IV collagen along the basal side of the epithelial flaps (Figure 5, *A*). Staining for type VII collagen was consistent with that of type IV collagen at all sites (Figure 5, *B*). Integrin α_6 had 2 distinct patterns in the epithelial flaps after mechanical separation. Continuous linear expression of integrin α_6 was seen beneath the basal epithelial cells in some regions,

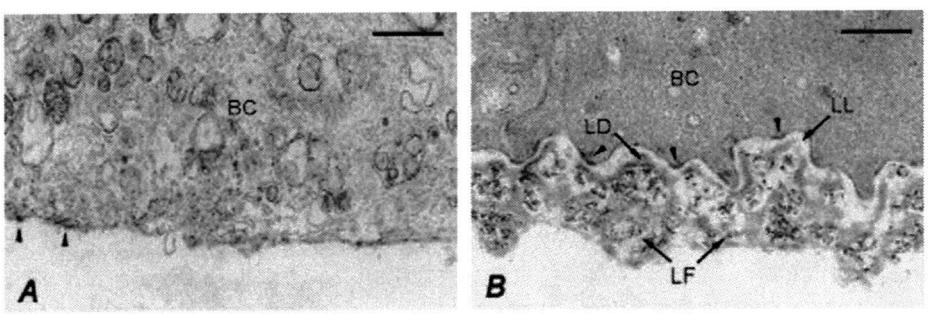

Figure 4. Transmission electron micrographs of epithelial flaps after mechanical separation. *A*: The epithelial flaps have no epithelial basement membrane. There are fewer hemidesmosomes (*arrowhead*) on the basal side of the epithelial basal cells (BC), which has several small intracellular blebs. *B*: The epithelial flap with the lamina lucida (LL), the lamina densa (LD), and part of the lamina fibroreticularis (LF). The cell morphology and intracellular structure of the basal cells (BC) are well preserved, and the hemidesmosomes (*arrowhead*) adhere to the basal lamina (*bars* = 200 nm).

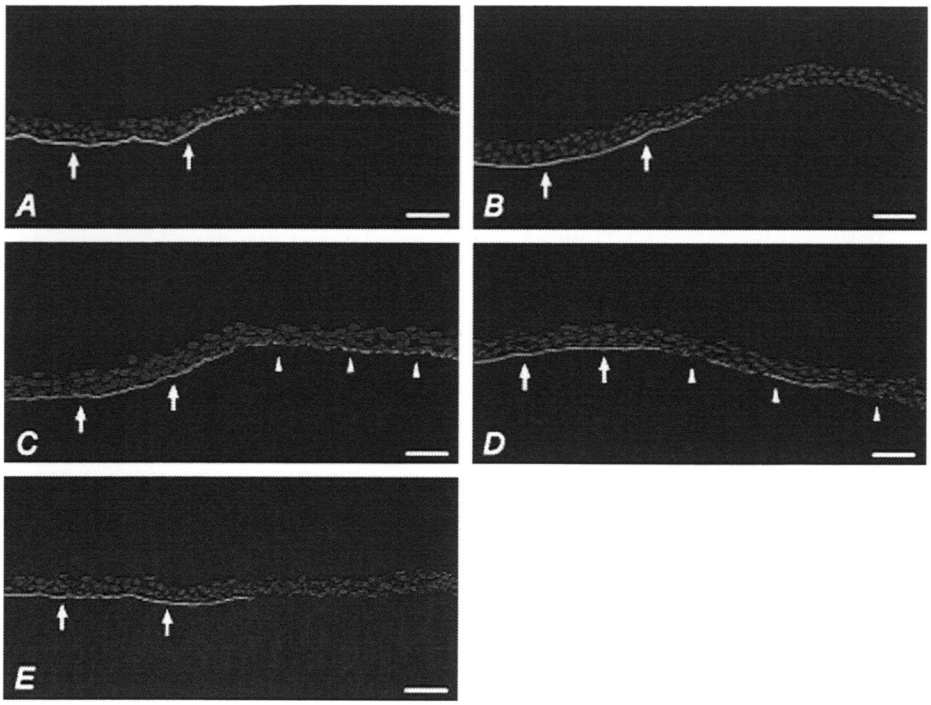

Figure 5. Immunostaining of an epithelial flap for types IV and VII collagens, integrin α_6 and β_4, and laminin 5. *A*: Discontinuous positive staining of type IV collagen along the basal side of the epithelial basal cells (*arrows*). *B*: Discontinuous positive staining of type VII collagen along the basal side of the epithelial basal cells (*arrows*). *C*: Linear staining (*arrows*) and patchy expression (*arrowheads*) of integrin α_6 along the bottom of the epithelial flap. *D*: Linear staining (*arrows*) and patchy expression (*arrowheads*) of integrin β_4 along the bottom of the epithelial flap. *E*: Discontinuous positive staining of laminin 5 along the basal side of the epithelial basal cells (*arrows*) (*bars* = 50 μm).

and inconsistent staining was observed in other areas (Figure 5, *C*). The staining patterns for integrin β_4 also had the 2 characteristic arrangements that were similar to those of integrin α_6 (Figure 5, *D*). Within the epithelial flaps, laminin 5 was expressed linearly along the basal side of the epithelial layers (Figure 5, *E*). These findings suggest that the cleavage plane of the epithelial flap was created within the lamina fibroreticularis in the regions of the positive staining for types IV and VII collagens, integrins α_6 and β_4, and laminin 5. In contrast, when epithelial separation was within the lamina lucida, no positive staining for types IV and VII collagens or laminin 5 was observed. The patchy staining of integrin α_6 and integrin β_4 suggests that epithelial flaps were not cleaved in the deeper regions of the lamina lucida but were cleaved only beneath the cell membrane of the basal cells.

Stromal Beds

Hematoxylin–eosin staining of the stromal beds showed that Bowman layer and the corneal stroma were well conserved after mechanical separation. All specimens also had smooth surfaces with no trauma to Bowman layer (Figure 6).

Scanning electron microscopy of the stromal beds at low magnification (×50) showed that the surface of the stromal beds was relatively smooth with little debris (Figure 7, *A*). High-resolution observation (×1000) of the surface of the stromal bed indicated that the exposed areas were mostly within Bowman layer; however, portions of the basement membrane were present in some regions (Figure 7, *B*). The 2 differing stromal surfaces were observed in all eyes. The regions of the stromal bed with portions of the basement membrane were generally seen as several island-like formations mainly in the center of the stromal bed, with the surrounding areas having mostly exposed regions of Bowman layer. At higher magnification (×10000), the anterior surface of the mostly exposed Bowman layer comprised a network of straight and curved fibers with some debris, which may have been part of the lamina fibroreticularis (Figure 7, *C*). In the regions with portions of the basement membrane, there were granular and amorphous components of the ECM on the surface of the basal lamina (Figure 7, *D*). At the

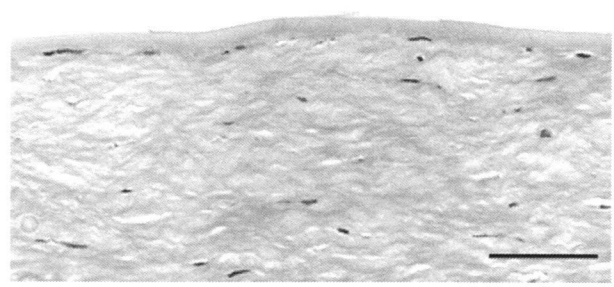

Figure 6. Light micrograph of a stromal bed after mechanical separation (*bar* = 50 μm).